Contrast agents for molecular photoacoustic imaging: current status and future potential

Judith Weber[1], Paul C Beard[2,*] and Sarah E Bohndiek[1,*]

[1] Department of Physics and Cancer Research UK Cambridge Institute, University of Cambridge, U.K.

[2] Department of Medical Physics and Biomedical Engineering, University College London, U.K.

* Corresponding Author information:

Professor Paul C Beard: Professor of Biomedical Photoacoustics. Department of Medical Physics and Bioengineering, University College London, Malet Place Engineering Building, London, WC1E 6BT, U.K.
Phone: +44 20 7679 0290; Fax: +44 20 7679 0255; Email: paul.beard@ucl.ac.uk.

Dr Sarah E Bohndiek: University Lecturer in Biomedical Physics. Department of Physics, JJ Thomson Avenue, Cambridge, CB3 0HE, U.K. and Junior Group Leader, Cancer Research UK Cambridge Institute, Li Ka Shing Centre, Robinson Way, Cambridge, CB2 0RE, U.K.
Phone: +44 1223 337267; Fax: +44 1223 337000; Email: seb53@cam.ac.uk.

Abstract

Photoacoustic imaging (PAI) is an emerging tool that bridges the traditional depth limits of ballistic optical imaging and the resolution limits of diffuse optical imaging. Using the acoustic waves generated in response to the absorption of pulsed laser light, it provides non-invasive images of absorbed optical energy density at depths of several centimeters with a resolution of ~100 μm. This versatile and scalable imaging modality has now shown potential for molecular imaging, which enables visualization of biological processes non-invasively using systemically introduced contrast agents. Understanding the relative merits of the vast range of contrast agents reported, from small molecule dyes, through gold and carbon nanostructures, to liposome encapsulations, represents a significant challenge. Here, we critically review the physical, chemical and biochemical characteristics of the existing photoacoustic contrast agents, highlighting key applications and also the present challenges for molecular PAI.

1. Introduction to molecular Photoacoustic Imaging (PAI)

Molecular imaging aims to visualize and quantify biological processes at the molecular and cellular level in a non-invasive manner, providing an opportunity to detect, stage, predict and monitor the development of disease. As early as the 17th century, Anton van Leeuwenhoek and Robert Hooke used light to visualize cells. For medical imaging, however, light suffers from significant scattering in biological tissue, which requires a trade off between depth of penetration and spatial resolution. Microscopy and other techniques that utilize unscattered photons can provide high resolution imaging (~1 μm) but only up to a depth of ~1 mm in most biological tissues; diffuse optical techniques such as fluorescence and near infrared optical tomography that exploit multiply scattered photons can provide penetration depths of several cm provided spatial resolution is sacrificed (>1 mm).[1]

Photoacoustic imaging (PAI) is an emerging method that combines the high contrast of optical imaging with the high spatial resolution of ultrasound.[2–4] Tissue heating due to the absorption of short laser pulses by endogenous chromophores or exogenous molecular imaging contrast agents produces broadband acoustic waves at MHz frequencies. These photoacoustic waves can be detected by ultrasound transducers at the tissue surface and reconstructed to form an image of the absorbed optical energy distribution. A brief explanation of the image formation process and required conditions for the image to represent absorbed optical energy can be found in Supplementary Note 1. Since sound waves are less scattered in tissue than photons, PAI can push the traditional limitations of optical imaging. For example, when operating in the 'near-infrared (NIR) window' (620 – 950 nm), tomographic PAI can reach a penetration depth of several cm with a resolution of the order of a few 100 μm, scaling to < 100 μm resolution for shallower (<1 cm) penetration depths.[2]

Chromophores (light absorbing molecules) intrinsic to living systems such as hemoglobin[5–7] and melanin[8,9], provide structural and functional information in PAI. Building on this intrinsic contrast with advances in exogenous contrast agents, PAI is currently one of the fastest-growing molecular imaging techniques. Given that molecular PAI is relatively affordable and portable, it has been rapidly incorporated for preclinical imaging *in vivo* in small animals for a range of disease indications. In this realm, the prevailing application by far is in cancer research, where PAI has been explored for: primary tumor detection and molecular characterization[10,11]; therapeutic monitoring[6]; as well as for the identification and assessment of metastatic lymph nodes[12].

This review highlights the latest advances in exogenous contrast agents for molecular PAI. After a basic introduction to the considerations needed for *in vivo* molecular PAI, including discussion of the background endogenous PA contrast, we detail the physical, chemical and biochemical characteristics of available contrast agents. Given the widespread use in cancer research to date, we draw on this research field for key examples of molecular PAI throughout the article. An overview of the strengths and weaknesses of each approach is provided in the outlook, to help guide new investigators in the field towards an appropriate contrast agent for their application.

2. Sources of endogenous contrast in PAI

While the focus of this review is exogenous contrast agents, it is important to appreciate the capabilities of, and challenges presented by, background endogenous PA signals when performing molecular PAI.

2.1. Intrinsic chromophores

Endogenous PAI provides structural and functional information through light absorption by hemoglobin, lipids, water and melanin (Fig. 1a). Hemoglobin, a protein composed of four heme-containing polypeptides residing in red blood cells, delivers oxygen throughout the body. The heme group is an iron-containing aromatic porphyrin ring system that is strongly absorbing and experiences structural and electronic modifications upon oxygen binding (Fig. 1b). The resulting change in the absorption spectrum (Fig. 1a) offers the prospect of measuring total hemoglobin concentration (Hb_{total}) and oxygen saturation (sO_2), important for non-invasive visualization of tumor angiogenesis (Fig. 1c).[5,6] PAI can also map lipid distribution *in vivo*[13] based on the absorption peaks at 930 and 1210 nm (second overtone of abundant C-H bonds), while water can be identified based on the absorption peak at 975 nm.[14] Melanin is a ubiquitous natural pigment in skin, hair and eyes, with intense optical absorption; while strong skin pigmentation may present a limitation as it reduces the amount of light penetrating deep into tissue, it does enable sensitive characterization of primary melanoma[15,9] and metastatic melanoma cells[16]. Nonetheless, these chromophores: probe only a limited range of biological processes; do not provide access to molecular information; and give a significant level of background absorption that must be accounted for when performing molecular imaging with exogenous contrast agents.

2.2. Genetically encoded chromophores

Most cells in the body are invisible to PAI in the NIR window. Reporter gene imaging enables visualization of the location and level of gene expression, promoter activity and protein-protein interaction in cells *in vivo* with PAI.[17] Under the control of the promoter of the gene of interest, a reporter gene expresses proteins that either provide PA contrast directly or create a product that yields PA contrast (Fig. 2a). Reporter genes are suitable for applications where the cell or biological process of interest does not provide inherent PA contrast but use of a contrast agent is undesirable, for example, in longitudinal studies of tumor development.

An example of a reporter gene system in which the expressed protein directly provides contrast is the genetically encoded green fluorescent protein (GFP) family of proteins.[18] The GFP family is, however, too blue-shifted for *in vivo* applications beyond virtually transparent organisms[18] due to strong background absorption by endogenous chromophores at visible wavelengths (Fig. 1a). Unfortunately, the GFP-like red-shifted fluorescent proteins exhibit limited PA signal generation efficiency and photostability.[19] The development of phytochrome-based NIR fluorescent proteins have begun to overcome these limitations[20,21] as they display a relatively low fluorescence quantum yield, making them ideal for PAI. Phytochromes are

photosensory receptors that absorb light when they covalently bind a linear tetrapyrrole chromophore, such as biliverdin. Since biliverdin is an intermediate of normal mammalian heme metabolism, phytochromes are promising candidates as PAI genetic reporters for *in vivo* imaging. The first example in this class was iRFP, which can be excited at ~690 nm and shows good photo- and thermo-dynamic stability *in vivo*.[21] More recently, differential imaging of the on / off states in the reversibly switchable phytochrome BphP1 has been demonstrated. Excitation of the biliverdin-BphP1 complex with light in the range of 730-790 nm triggers the bound biliverdin to switch from trans to cis conformation (Fig. 2b), causing a change in the absorption spectrum towards 630-690 nm.[22] The photoconversion was shown to reduce the impact of background signals (Fig. 2c), improve detection sensitivity and increase penetration depth. Reversibly switchable phytochromes may therefore play a significant role in future preclinical research studies, for example, in localizing tumor development in transgenic mouse models in deep tissue.

More widely explored transgenic approaches for PAI are based on enzymatic reporter genes. Here, the genetic product is an enzyme that produces a chromophore or its precursor. Enzymatic reporter genes can amplify signals as one enzyme can interact with many substrates. LacZ is a bacterial gene that encodes the enzyme β-galactosidase, which catalyzes the hydrolysis of lactose into galactose and glucose. For PAI, a lactose-like substrate, 5-bromo-4-chloro-3-indolyl-β-D-galactoside (X-gal), is added.[23] X-gal is transparent but upon metabolism a stable dark-blue product emerges. Dual-wavelength PAI can detect tumor cells expressing lacZ up to 5 cm depth with high resolution.[23] The lacZ-reporter gene system is limited, however, as X-gal must be locally administered and the metabolic product shows poor clearance. The tyrosinase-reporter gene system (Fig. 2d,e) introduces the key enzyme in melanin synthesis into non-melanogenic cells, hence does not require an exogenously administered substrate.[24] Although the relatively featureless absorption spectrum of melanin (Fig. 1a) could make it hard to distinguish from intrinsic signals, *in vitro* and *in vivo* PAI of tyrosinase-expressing cells has shown high sensitivity[24,25] and inducible systems can address potential toxicity concerns.[26] Despite their potential for signal amplification, the enzymatic reporter systems are generally less desirable due to their lack of product specificity, as well as dependence on metabolic activity of the cells and substrate availability, which limits quantification.

3. Exogenous contrast agent considerations for molecular PAI

To perform molecular imaging, we create a contrast agent composed of a signaling compound, which produces the signal for imaging, and a targeting moiety that enables the readout of a specific biological process of interest (summarized in Fig. 3).

3.1. Photophysical properties: signaling compounds

The ideal signaling compound, which is the substance or label that provides the PAI signal, needs to exhibit the following characteristics: high molar extinction coefficient (Fig. 4), to maximize the amount of light absorbed; sharply peaked characteristic absorption spectrum, to ensure unambiguous identification by spectral unmixing even at low molar concentrations (see Supplementary Note 1); peak absorption in the NIR window (620 – 950 nm), to maximize penetration depth by avoiding the strong absorption of intrinsic chromophores (Fig. 1a); high photostability, to ensure that spectral features are not changed by light irradiation; low quantum yield, to maximize the non-radiative conversion of light energy to heat; and efficient conversion of heat energy to stress[2], to produce acoustic waves.

Signaling compounds that begin to fulfill the above criteria and can be sensitively detected using PAI are now available. These fall into three broad classes: small molecule dyes; metallic or semiconducting nanostructures; and organic nanostructures (Fig. 3). The resulting contrast agents (signaling compound + targeting moiety) must also overcome physiological barriers to reach the target, while ensuring biocompatibility for *in vivo* imaging, as discussed in the following section.

3.2. Biological properties: targeting and biocompatibility

The targeted molecular imaging contrast agent must overcome circulatory and cellular barriers (Fig. 5). Initially, the interaction of the contrast agent in the bloodstream must be carefully considered. For example, it is now clear that due to their high surface free energy, nanoparticles rapidly (within < 30 s) adsorb biomolecules when in contact with biofluids.[27,28] The resulting 'protein-corona' is highly complex and functionally diverse, varying significantly between different nanoparticles.[27] The presence of a protein-corona influences immune response and target binding[28,29], which has led some investigators to suggest biological responses to nanoparticles *in vivo* reflect the nature of the adsorbed layer rather than the nanoparticle itself[28].

Assuming we can characterize the nature of the contrast agent interactions with the bloodstream[27,28] the next stage is to pass out of the circulatory system. To extravasate, a maximum size limit of typically < 10 nm is necessary, although for applications in cancer, contrast agents of up to 100 nm have been found to pass through the leaky and immature vasculature[30]. Once in the tissue interstitium, passing the cellular barrier can be achieved by active targeting, for example to cell surface receptors[31], transporters[32], metabolic enzymes[33] or biochemical processes[34], or by relying on passive uptake through diffusion or endocytosis.

To facilitate active targeting, the biological target should be (over)expressed at a very early stage of the disease and found at low levels in off-target tissues. Structures that can be used to achieve active targeting include small molecules, peptides and adhirons[35], affibodies[36], aptamers[37] and proteins; these are illustrated and reviewed in Figure 3. In particular, consideration must be given to biocompatibility, which refers here to minimizing toxicity (e.g. according to required administration route and dose) and immune response (e.g. by reducing accumulation in non-targeted tissue), as well as optimizing target tissue penetration and elimination from the circulatory system.

For example, using small molecules for targeting enables the contrast agent to pass physiological barriers easily due to their small size (< 1 nm) and clear rapidly through the kidneys, which reduces off-target accumulation and optimizes biocompatibility. Conversely, although proteins (e.g. monoclonal antibodies) show high target affinity and specificity, and thus display little cross-reactivity with healthy tissues, their larger size results in poorer tissue penetration and clearance, and immunogenicity is possible, resulting in poorer biocompatibility. Antibody fragments, such as diabodies, are now being developed to address these challenges, since they are smaller in size but retain high affinity and selectivity.[36,38]

As noted above, for cancer research, the hyperpermeability of tumor vasculature combined with the lack of an intact lymphatic drainage may lead to 'enhanced permeability and retention' (EPR) of contrast agents of up to ~100 nm inside the tumor tissue without the need for targeting ligands.[39] 'Passive' targeting based on the EPR has been demonstrated extensively in mice (see Supplementary Tables) and recently the first studies have begun to emerge in humans[40]. This passive approach can be applied to aid tumor localization. Larger entities (> 100 nm) are typically not accumulated and will be cleared through the reticuloendothelial system.[30] From the perspective of molecular PAI, however, passive targeting confounds attempts to perform targeted molecular imaging, as uptake is not specific to a biological process hence should be avoided as far as possible by contrast agent design.

4. Signaling compounds for molecular PAI

A catalogue of exogenous contrast agent studies using PAI for the different classes of signaling compounds can be found in Tables S1-S4 and associated references. Figure 4 enables direct comparison of two critical parameters for the ideal signaling compound: the specific extinction coefficients and peak absorption wavelengths for the different classes. While small molecule dyes are generally commercially available, this is not often the case for nanostructures, so we refer the reader to Supplementary Note 2 for further information regarding common chemical synthesis routes for each class of nanostructure reviewed here.

4.1. Small molecule optical dyes

Small molecule optical dyes (Table S1) have optimal biocompatibility (good tissue penetration and rapid clearance) compared to all other molecular PAI contrast agent classes due to their small size (<2 nm). However, they also possess the poorest molar extinction coefficient and often exhibit relatively low photoacoustic generation efficiency and photostability. The chemical basis of these dyes is a series of conjugated double-bonds and/or (mostly aromatic) ring systems. In these highly conjugated structures, electrons are delocalized meaning less energy is needed for excitation. The well-defined energy gap between ground and excited states results in a distinct, albeit relatively broad, absorption peak (Fig. S1). Relaxation of the excited electrons can occur in radiative (fluorescence or bioluminescence) or non-radiative processes, dependent on the lifetime and electronic configuration of the excited states (Fig. 6a).[41] For PAI, a large non-radiative relaxation is required so the quantum yield (referring to fluorescence emission) should be as low as possible.

The first main class of NIR dyes used for PAI is the heptamethine cyanine dyes. They comprise two aromatic nitrogen-containing heterocycles linked by a heptamethine chain and their synthesis is well established.[42,43] For example, indocyanine green (ICG) is an FDA approved dye with low toxicity. High hydrophobicity results in high plasma protein binding, hence it has been used in the clinic for over 35 years as a blood flow contrast agent.[44] It has an absorption maximum at 780 nm (in aqueous solution) and a relatively low quantum yield for fluorescence (0.027 in aqueous solution) yielding PA signal.[45] While ICG has been used as a perfusion marker in PAI for functional imaging[5], the inherent hydrophobicity results in significant variations in the optical properties dependent on the concentration and environment (Fig. 6b)[46] and targeting chemistry is difficult, meaning unmodified ICG is not ideal for molecular PAI.[47,48] There is the prospect of addressing these limitations via modifications, such as the integration of a cyclohexenyl ring in the methine linker, which can increase photostability and enable further chemical modifications for targeting.[43]

Squaraines are the second main class of NIR dyes that could be employed for molecular PAI. They are characterized by an electron deficient central 4-membered ring often conjugated to two electron-donating groups to generate a donor-acceptor-donor form, which increases the delocalization of the electrons. The optical properties can be tuned by varying donor strengths to produce sharp absorption bands in the NIR range.[49] Despite good optical properties and

photostability, squaraines are often limited by insolubility, aggregation and chemical reactivity.[50,51] In PAI they have only been used in conjunction with phospholipids, albumin or polymers (see Section 4.2.3) owing to poor solubility.[52–54]

The two water soluble, FDA-approved azo dyes, methylene blue (MB) and Evans blue (EB), with absorption peaks at 664 nm (MB) and 620 nm (EB), have also been used for PAI but are limited at depth as their absorption peak is at lower end of the NIR range.[55,56] Characteristic for MB is its long triplet state lifetime and a high quantum yield for triplet state transition, which can be used for PA lifetime imaging.[55] Although most NIR dyes are benign *in vivo*, MB can cause photodamage under intense irradiation and chemical side effects due to reactions with cellular molecules (e.g. NADH, FADH),[57] making it less desirable.

Given the existing FDA approval of ICG, MB and EB as blood flow agents, they were quickly applied in cancer research studies using PAI for identification of the closest lymph node in the drainage path from a tumor[58–60], the sentinel lymph node (SLN). This process is crucial in TNM clinical cancer staging. However, as an example of the limitations of passive targeting, SLN identification with dye molecules has shown a relatively high false positive rate.[61]

Most small molecule dyes must be actively targeted to gain specificity. A common target for detection and characterization of solid tumors in preclinical research is the cell surface epidermal growth factor receptor (EGFR). EGFR is frequently overexpressed in solid tumors, including breast and pancreatic tumors, contributing to uncontrolled cell proliferation. Several successful targeted cancer therapies (e.g. cetuximab, gefitinib, erlotinib) function by inhibiting EGFR[62,63], hence imaging the expression of EGFR within a tumor could help select patients for such therapy and monitor their response. Hudson *et al* explored the potential of molecular PAI for this application in an orthotopic mouse model of pancreatic cancer (depths >5 mm) by conjugating the epidermal growth factor (EGF) protein to the NIR dye CF-750 (Fig. 6c).[64] The absorption spectrum of CF-750 was not significantly altered by the bioconjugation to EGF and the probe signal could be clearly distinguished from background by multi-wavelength PAI, providing a non-invasive readout of EGFR expression. Importantly, there was no noted toxicity.

4.2. Nanostructures

Nanoparticles (NPs) embody the largest class of contrast agents for molecular PAI. They possess high chemical, physical and biochemical flexibility, as well as significantly increased molar extinction coefficients compared to small molecule dyes. NPs exist in different materials, shapes and sizes (< 1000 nm, usually ~10-100 nm), and have tunable surface properties, reactivity and optical characteristics. Their large surface area enables signal amplification as the large number of targeting moieties that can be attached per particle increases the target-binding probability. However, due to their larger size, NPs often accumulate in the reticuloendothelial system for long time periods, yielding poorer biocompatibility. Furthermore, the reproducibility, purification, and quantification of homogeneous NP preparations remains challenging.[65] Details of the synthesis routes that are currently used to define optical properties for all nanostructures (metallic, semiconducting and polymer) are given in Supplementary Note 2, while reports of alternative

nanomaterials including perfluorocarbon, iron oxide and copper sulfide are detailed in Supplementary Note 3.

4.2.1. Gold

The main focus of research into metallic nanoparticles for molecular PAI has been on gold, owing to its unique optical and physicochemical properties, relatively inert nature, and prior use in humans (for example, in treatment of rheumatoid arthritis and dental fillings). In addition, gold forms strong gold-thiolate bonds that enable covalent surface modifications for optimizing biocompatibility (e.g. poly(ethylene glycol) (PEG) functionalization)[66], stability (e.g. silica encapsulation)[67] and active targeting (conjugation to ligands as in Fig. 3).

The optical properties of GNPs arise from the 'localized surface plasmon resonance' (LSPR) phenomenon. The conduction electrons of a GNP oscillate relative to the atomic core when exposed to light of an appropriate wavelength (Fig. 7a). This state is referred to as plasmon.[68] Plasmons convert a significant part of the oscillation energy into heat detectable with PAI. The key advantage of GNP for PAI signal generation is that they essentially act as a macroscopic dipole, leading to an extinction coefficient several orders of magnitude higher (Fig. 4) than small molecule dyes (extinction scales ~ volume^3).[69]

The frequency of the LSPR determines the peak absorption wavelength of the GNP, which can be tuned based on: size (surface-to-volume ratio); polarization modes; edge / vertex number and 'sharpness' of the GNP. Therefore, in addition to spheres, a wide range of GNP shapes, including stars, tripods, plates and prisms have emerged (Table S2). One key example of tuning is found in gold nanorods (GNRs), whose intense and narrow LSPR absorption bands in the NIR are tuned by varying their aspect ratio (Fig. 7b, Supplementary Note 2.1). Under laser illumination for PAI, larger GNRs may not be thermodynamically stable[70] and can collapse to spherical GNPs or fragment / sublime. Silica encapsulation has been found to improve photostability[71] by increasing thermal conductivity to the surrounding medium, which also increases PA conversion efficiency.[67,72] A second key example is the use of hollow gold nanostructures, such as gold nanocages (GNCs) and gold nanoshells (GNSs) that can encapsulate cargo such as drugs within their porous walls for theranostic purposes (see Section 5). The LSPR frequency can be conveniently tuned not only based on size but also on shell thickness (thinner = red shift) (Fig. 7c).[73,74] These simple methods for tuning the characteristic spectral shape and peak wavelength are highly advantageous for molecular PAI.

Active targeting of GNRs has been demonstrated through antibody conjugation (Table S2) although it is more challenging than for small molecule dyes due to the larger size of the GNR relative to physiological barriers. Due to their relatively narrow spectrum, GNRs tuned to absorb at a range of different peak wavelengths can be conjugated to multiple targets, which has enabled multiplexed characterization of tumor EGFR and human epidermal growth factor receptor 2 (HER2) expression, allowing characterization of heterogeneous tumors[11] and potentially enabling specific tracking of combination therapies.

In addition to cancer cell receptors, an alternative approach for tumor targeting is specific imaging of the angiogenic tumor vasculature (in contrast to quiescent surrounding vessels) by targeting $\alpha_v\beta_3$ integrin, which is overexpressed on

angiogenic blood vessels. Targeting the vasculature removes the physiological barrier of extravasation in molecular imaging. The tripeptide arginine-glycine-aspartic acid (RGD) and its derivatives are widely used targeting moieties. All reports to date use a bifunctional PEG linker to conjugate the GNP with the RGD derivative (Table S2). Studies with larger RGD-modified GNPs suffer from high accumulation in the reticuloendothelial system and slow tumor accumulation of at least 6 h.[31,75] This is unfavorable in terms of biocompatibility, as it renders the reticuloendothelial system organs prone to, for example, oxidative damage via free radical formation.[76] These limitations were recently overcome using small gold tripods (< 20 nm) conjugated to the RGD derivative cyclic Arg-Gly-Asp-D-Phe-Cys via a PEG linker (Fig. 7d, e), obtained in high yield with narrow size / shape distributions and, due to their PEG-coating, excellent stability.[77] PAI results were verified with ^{64}Cu PET. Encouragingly, RGD-gold tripods showed rapid tumor accumulation within 2 hours (subcutaneous U87MG in mouse) without systemic toxicity. While preclinical GNP studies generally show low acute toxicity, *in vivo* biocompatibility needs to be more systematically addressed through longer term toxicity studies for each nanostructure to establish the impact of these non-biodegradable NPs.

4.2.2. Carbon

Carbon forms different allotropic structures: carbon nanotubes, graphene-based nanomaterials and nanodiamonds. All three classes can be synthesized to possess an intrinsic absorption in the NIR range (Fig. 8, Fig. S2, Supplementary Note 2.2) and thus play an important role for PAI (Table S3). Despite possessing a lower molar extinction coefficient than gold, carbon nanoparticles (CNPs) hold significant potential for molecular PAI due to their flexibility of synthesis and functionalization (Supplementary Note 2.2). Of particular interest is the wide variety of covalent[78–81] as well as non-covalent modifications with small molecules (dyes[82], drugs[83], surfactants[84]), polymers[82] and biomolecules[85] that can be used for: targeting; increased solubility and stability[86]; improved signaling properties[87], increased specificity[82]; or for theranostic approaches[88]. The absorption spectra of CNPs tend to be relatively broad in the NIR range, presenting a challenge for spectral unmixing in molecular PAI, but the attachment of NIR dyes can circumvent this limitation (Fig. S3).

The majority of molecular PAI studies using carbon have been performed using single-walled carbon nanotubes (SWNT). SWNTs can be visualized as cylindrically rolled-up graphene sheets with diameters of 1-3 nm and lengths up to centimeters (Fig. 8a).[89] Semiconducting SWNT exhibit numerous optical absorption peaks of relatively similar magnitude (Fig. 8b,c). The absorption peaks are defined by narrow energy ranges where many electronic states are available (referred to as van Hoff singularities, Fig. 8b). The electronic, and thus optical, properties are tunable by changing the tube structure, for example, diameter and chirality. The bandgap generally varies inversely with the diameter, but many open questions remain regarding the complex photophysics of SWNTs.[90,91]

Molecular targeting of the $\alpha_v\beta_3$ integrin for angiogenesis imaging has been achieved in multiple studies of CNPs using RGD-peptides attached to SWNT.[82,92–94] De la Zerda *et al* conjugated RGD peptides through PEG grafted phospholipids to

SWNT. *In vivo* evaluation found a strong PAI signal in the tumor for SWNT-RGD compared to only weak signals (via passive EPR uptake) for non-targeted SWNTs.[92] Attachment of NIR dyes to the surface of the nanotubes achieved over 100-times higher PA contrast and sub-nanomolar sensitivities in mice compared to plain SWNT.[82,94] However, the extent to which the improved sensitivity was due to synergistic quenching effects between the dyes themselves or between the dyes and the SWNT was not established. In addition, photobleaching can occur due to the instability of the dyes associated with these constructs.

SWNTs have also been specifically targeted to tumors overexpressing the cell surface glycoprotein CD44, which has been implicated in many tumor hallmark processes including cell proliferation and migration. Targeting of CD44 has been considered for both diagnosis and therapy of the disease.[95] Coating SWNT with a hyaluronic acid-based biosurfactant acts as targeting moiety to CD44. The coating is degraded by enzymes (hyaluronidases) overexpressed in cancer cells. Further labeling of the hyaluronic acid-unit with a fluorescent dye has been used to provide validation of the selective CD44 receptor uptake using PAI and fluorescence imaging (Fig. 8d, e)[86] illustrating controlled SWNT delivery.

Several studies have reported cytotoxicity and inflammatory potential of SWNTs[96,97] that can be significantly reduced by functionalization.[98,99] On the contrary, emerging evidence suggests that nanodiamonds exhibit high biocompatibility[100,101,102], which makes them a promising new molecular PAI contrast agent. As for GNPs, the biological impact of CNPs is dependent on the surface modification, size and synthesis method.[103] Significant future effort will need to be invested to better understand CNP photophysics and biocompatibility, in order that their highly flexible functionalization and tunable optical properties can be fully exploited for molecular PAI.

4.2.3. Organic Nanostructures

An exciting recent development in molecular PAI is the use of polymer nanoparticles and encapsulations (Table S4). They have a high structural and functional flexibility (composition, shape, charge, size) and for molecular PAI act: a) directly as signaling compounds; b) to enhance the biocompatibility of other signaling compounds; or c) as a foundation for activatable imaging probes. The most popular organic polymer structures used for PAI contain either conjugated polymers or porphyrin related units, such that they directly absorb light. Their molar extinction coefficient sits between the small molecule dyes and GNPs (Fig. 4), and while their absorption spectra may be broad (Fig. 9a), they usually exhibit a well-defined absorption peak in the NIR and are also relatively photostable. Furthermore, the chemically and physically stable polymeric platform provides the opportunity to attach specific targeting and therapeutic moieties (see Supplementary Note 2.3) and may yield favorable biocompatibility, although this has yet to be established.

Polymer nanoparticles come in many different flavors. Conjugated polymers (CP) are macromolecular structures with a highly delocalized conjugated backbone (Fig. S4a). In contrast to small molecule NIR dyes, the conjugated system is spread through the entire polymer backbone and the polymers are densely packed into NPs yielding high absorptivity and photostability. The optical properties (strongly dependent on the conjugated core) can be tuned by adopting different backbone

structures, combining different conjugated polymers and controlling aggregation and surface functionalization.[104–106] As an example, polypyrrole NPs are advantageous for PAI due to intense NIR absorption, high photothermal conversion efficiency and good biocompatibility even though their absorption spectrum is relatively featureless.[107] They can be well dispersed in aqueous solution and biocompatible due to their small size (<50 nm) and hydrophilic surface coating.[107] However, they lack functional groups for surface modification, so alternative CPs that can be enriched with functional units are being developed.[108,109] These alternative CPNPs are characterized by high photostability and an alternating electron donor-acceptor structure, which increases the delocalization of the electrons in the conjugated system, shifting the absorption spectrum towards longer wavelengths (Fig. S4b). Compared with SWNTs and GNRs they also have been shown to yield 4-fold higher PAI signal *in vivo* on a per mass basis, but lower than the GNRs when compared on a molar basis.[109] They have also facilitated the development of a 'smart' contrast agent (see Section 5) for *in vivo* real-time imaging of reactive oxygen species.[109]

Alternatives to synthetic CPs are the naturally occurring porphyrins, aromatic macrocycles from heme and chlorophylls containing four pyrrolic units linked by methane (Fig. S4a). The chemical reactivity of the porphyrin macrocycle offers architectural flexibility, which permits tuning of the optical properties (Fig. S4b). As with uncoated CPNPs, porphyrins are extremely insoluble. Lovell *et al* overcame this challenge by conjugating porphyrin to a phospholipid, which resulted in self-assembled porphysomes with a bilayer structure.[110] The porphyrin molecules inside the porphysome create J-aggregates, red-shifting the absorption peak (Fig. S4b), and causing fluorescence quenching to yield a strong NIR PA signal.[111,110] The porphyrin-lipid shell was also used for encapsulation of carboxyfluorescein, doxorubicin[110] or fluorinated gases enabling multimodal PAI, US and fluorescence imaging.[112,113] As natural products, poryphyrins and porphysomes would be expected to show high biocompatibility, but due to their relative immaturity as contrast agents, this has yet to be established *in vivo*.

Other polymers lacking intrinsic optical absorption but showing favorable biocompatibility can incorporate added signaling compounds through micellar or vesicular structures. Liposomes have already been used in the clinic as drug delivery vehicles, providing a promising route towards clinical application.[114] Gold nanobeacons are formed from small GNPs (2-4nm) trapped within synthetic or natural amphilines, forming NPs 60 – 260 nm in size.[115,116] Advantages of such formulations include improved photo-stability, biocompatibility, signal intensity and targeting ability, relative to the signaling compound alone. Disadvantages include the presently limited knowledge of how polymer NP structure and local signaling compound concentration influences PA signal generation, as well as the larger size of the encapsulation.

Despite their early stage of development, polymers and encapsulations have been demonstrated in numerous passive targeting applications: imaging mouse brain vasculature[107,117] and tumor sentinel lymph node identification[109,118,110] as well as primary tumor characterization[119–121]. Conjugation of polypyrrole NPs to folic acid has recently been shown to actively target folate receptor positive (FR+ve) MCF-7 breast cancer xenografts (Fig. 9b, c). Biocompatibility was assessed only in cells *in vitro*; studies *in vivo* were limited to evaluating biodistribution, which showed the expected involvement of the reticuloendothelial system in contrast agent

clearance.[108] Wang *et al* exploited the same target with poly(D,L-lactide-co-glycolide) (PLGA) lipid NP doped with ICG. Both PLGA and ICG are FDA approved and the fabricated NPs showed good stability, high folate-receptor targeting efficiency and good PA signal *in vitro* and *in vivo* in the same model.[122] This shows promise for clinical translation, although it should be cautioned that FDA approval of the individual elements would not necessarily speed up approval of the newly synthesized product.

5. Emerging concepts in molecular PAI

Smart (or 'activatable') contrast agents elicit a prescribed signal change, such as a shift in the peak absorption wavelength, in response to a biological stimulus of interest. As well as increasing the range of possible molecular imaging targets, a key advantage of smart contrast agents is that they minimize the influence of the background signal from endogenous chromophores such as hemoglobin, hence offering a potential for high sensitivity of detection. The dynamic response of smart contrast agents also facilitates the study of processes such as enzymatic activity in real-time. Although relatively few examples exist so far for PAI, targeting proteases including matrix metalloprotease[10] and furin[33] has proven popular. Proteases are implicated in a range of disease processes, including tumor invasion and metastasis. In 'smart' contrast agents, the protease substrate (a short peptide) links a quencher (BHQ3) with either a fluorophore (Alexa750)[10] or NP (CuS)[123]. PA images acquired at the peak wavelengths of the two absorbers both show strong signals before the contrast agent reaches the target. Inside the tumor microenvironment, proteases cleave the linker, leaving one absorber that is targeted to reside in the tumor while the other absorber is cleared. Only one absorption peak is thus detected after cleavage, yielding a highly specific imaging approach to quantify protease activity non-invasively. Undesirable toxicity in off-target tissues with high physiological protease levels has yet to be assessed.

Multifunctional contrast agents can enable imaging of targets with different imaging modalities simultaneously ('multi-modality') or also deliver therapeutics ('theranostic'). Using multi-modality contrast agents it is possible to image the same target with two or more approaches (overcoming weaknesses of each modality) or to readout multiple targets, building a more complete picture of the underlying biochemistry. Molecular imaging modalities can differ in sensitivity up to 6 orders of magnitude[124] requiring a difficult compromise to satisfy the concentration requirements for each modality. While PAI has been combined with PET[77] and/or MRI[125,126] for whole body imaging to determine contrast agent biocompatibility, its natural partners are ultrasound and fluorescence imaging due to the acoustic detection and optical excitation paths. Several PA-contrast enhanced US contrast agents are available. Small molecule dyes used for PAI are also fluorescent. The motivation for combined fluorescence imaging is clear for surgical interventions: the increased depth penetration of PAI enables identification of the target with high spatial resolution, while real-time intraoperative tumor resection guidance is easily provided by fluorescence detection, avoiding the need for acoustic coupling of the PAI probe.[127]

Theranostic approaches link the disease diagnosis directly to therapy. The final aim is to create a safer, more efficient and tailored treatment aligned with the

concept of precision medicine. *In vivo* use of theranostic agents will help to better quantify target-specific delivery of the drug and controlled release[128] However, defining the distribution and effect of the therapeutic after release from the conjugate or carrier remains challenging, as do the opposing requirements of imaging agents and therapeutics including dosage and accumulation time.[129] A key example of theranostics with PAI is the use of photothermal therapy and photoactivated drug release in cancer. Exploiting the strong optical absorption and thermal conductivity of gold[125], carbon[130] and CuS[128,131] nanostructures, initial reports have shown promise but further work is needed to assess the true benefit of such combinations.

6. Outlook: Promise and future challenges

Molecular PAI is an exciting new modality that enables simultaneous imaging of endogenous chromophores in target cells and exogenous contrast agents that provide visualization of dynamic biological processes. In addition to using non-ionizing radiation and imaging in real-time with high spatial resolution, the technology also has the potential for relatively low cost implementations. While a broad range of application areas for molecular PAI have been identified, including oncology, neuroscience and cardiovascular diseases, basic research studies and preliminary clinical trials have focused primarily thus far on detection, staging and therapeutic monitoring in cancer.

6.1 How do we identify the most suitable contrast agent for a given molecular PAI application?

As reviewed in Section 3, development of a new contrast agent for molecular PAI requires consideration of both photophysical (optical and thermodynamic) and biological properties. Here we summarize these properties for each reviewed contrast agent class.

6.1.1 Small molecule dyes

With respect to the photophysical properties of the signaling compound, dyes typically exhibit a relatively low molar extinction coefficient ($<3x10^5$ M^{-1} cm^{-1}). They can also lack photostability or solubility and tend to aggregate. This intrinsic hydrophobic conjugated structure can lead to concentration- and environment-dependent spectral changes, which may make them difficult to detect *in vivo*. It is possible to address some of these challenges chemically, by attaching hydrophilic groups, introducing triplet-state quenchers[132] and integrating stabilizing groups[133]. Additionally, variations in the chemical design, such as varying the size of the conjugated system, attaching electron donating / withdrawing groups, allow tailoring of the spectral range. Their chemical flexibility also facilitates the creation of 'smart' contrast agents, which can in part compensate for their low molar extinction coefficient by minimizing the influence of the background signal from endogenous chromophores.

For molecular imaging, when combined with small targeting moieties, dyes can easily pass physiological barriers and be actively transported into cells. They are

rapidly cleared through the kidneys, which leads to a short blood half-life, minimal off target accumulation and hence favorable biocompatibility. The short half-life, while favorable for imaging perfusion, can present a challenge for molecular imaging studies as it limits the time for which the dye will circulate and hence accumulation at the target site.

On balance, in spite of their limitations, small molecule dyes remain good candidates for molecular PAI in the preclinical study of extravascular targets due to their small size, favorable biocompatibility and the ability to engineer 'smart' responses.

6.1.2 Gold nanoparticles

GNPs show the highest extinction coefficient in the NIR range and high PA conversion efficiency. Their narrow absorption spectrum can be tailored by tuning the LSPR using the size, thickness, edge number and sharpness of the GNP. These properties, along with surface coatings, can also be used to maximize photostability. GNPs therefore possess the most flexible photophysical properties of the compounds reviewed. Furthermore, easy and stable functionalization of GNPs can be made via gold-thiolate bonds, making them suitable for attachment of a range of targeting moieties and further signaling compounds for multimodal imaging. Their associated spectral flexibility means GNPs are highly suitable for multiplexed imaging of different targets within the same tissue.

In diseases that exhibit a leaky vasculature, like cancer, GNPs can be accumulated via the EPR effect (discussed in Section 3). Active targeting of GNPs to cell surface receptors has only been demonstrated in a limited number of cancer-related applications; it remains to be seen whether the use of GNPs in reaching extravascular targets generalizes across disease types and to other applications. Interaction of the GNPs reviewed here within the vascular and tissue compartments depends on their size, shape, charge and synthesis route. Hence, despite prior use of colloidal gold for therapeutic applications, for longitudinal monitoring studies requiring repeated contrast agent administration, biocompatibility *in vivo* may still present challenges since gold is not biodegradable.

6.1.3 Carbon nanoparticles

High photostability along with versatile methods of surface modification and functionalization make CNPs attractive for molecular PAI. CNPs come in three flavors: graphene nanosheets are zero band gap semiconductor with broad and flat absorption spectrum; semiconducting SWNT have a more specific absorption profile modified by tube diameter and chirality; carbon nanodiamonds can have high and specific NIR absorption depending on vacancies in the diamond crystal lattice. The photophysical properties of CNPs are generally limited by their relatively broadband absorption profile as well as low molar extinction coefficient (similar to dyes). It is possible, however, to address these limitations at least in part by conjugation of small molecule dyes to the SWNT and tuning of nanodiamond vacancies.

Current evidence as to the biocompatibility of CNPs is relatively limited but suggests that size and shape play a role (as with GNPs). Nanodiamonds may be most promising for preclinical studies, as they appear to lack toxicity based on *in vitro*

experiments. Systematic studies are required nonetheless to assess acute and long-term toxicity *in vivo*. Should these prove promising, the flexible physicochemical properties make CNPs an attractive target for future contrast agents.

6.1.4 Polymers and encapsulations

Conjugated polymers and porphyrin-based nanostructures can provide strong optical absorption due to the presence of highly delocalized electrons in the conjugated system, which is higher than both small molecule dyes and CNPs reported to date. Changing the delocalization degree of these electrons through electron donating / withdrawing groups and the inter- and intra- chain interactions can influence their photophysical properties.

The stable polymeric platform provides an opportunity to attach not only active targeting moieties but also drugs for theranostic applications and activatable functionalities for smart probes. Given that this class of contrast agents is relatively new, detailed biocompatibility studies are still lacking to prove their potential for *in vivo* application. However, water-soluble, organic polymeric structures such as liposomes (that lack intrinsic optical absorption but are already clinically approved) have been combined with other signaling compounds to create a polymeric contrast agent with known biocompatibility.

Polymers and encapsulations represent a growing field in molecular PAI, with exciting potential for theranostics given their high functional flexibility. Further work to develop biocompatible platforms with even higher NIR absorption is expected to emerge in the coming years.

6.2 How do we facilitate uptake of molecular PAI in basic research?

Despite great progress in molecular PAI contrast agent development in recent years, several challenges must be overcome in order to facilitate uptake into basic research in the life sciences. It is crucial that the field recognize the need for standardized reporting of experimental approaches, for example, with regard to the measured photophysical properties. Publications should report in detail their calculations of extinction coefficients on both a ‘per mass’ and ‘per mole’ basis, along with independent measurements of both optical and photoacoustic absorption spectra as a function of concentration and solvent. Such data has a major impact on biocompatibility since detection sensitivity is intrinsically linked to dosing *in vivo*. Systematic studies to improve solubility, stability and specific targeting capability would be highly advantageous in this regard, as would reproducible, cost effective and scalable chemical syntheses and purification methods.

With photophysical and chemical characteristics optimized, criteria related to targeting and biocompatibility must also be fulfilled. Relatively few studies have shown convincing evidence of active targeting, for which cellular controls (e.g. knockdowns) and physiological controls (e.g. blocking) are needed. The large size of nanostructures relative to physiological barriers may limit their application to intravascular targets for molecular imaging outside of cancer. Although the materials reviewed here are often claimed to be inert, biocompatibility appears to be strongly dependent on the nanostructure size, shape and synthesis method used in their preparation. Biological interactions, immunogenicity, stability, circulation and target

tissue retention must therefore be well characterized to define the safety profile of the contrast agent on a case-by-case basis. Recent studies tend to consider *in vivo* biodistribution and *in vitro* toxicity but rarely combine both. Therefore, going forward, biocompatibility of different contrast agents has to be better evaluated at the cellular and organismal levels (both through blood sampling and tissue analysis) to identify potential acute and chronic inflammatory and toxicity effects.

With biocompatibility concerns addressed, molecular PAI then has to achieve technical and biological validation before acceptance as a routine tool. Technical validation requires assessment of precision (repeatability / reproducibility) and accuracy (ability to relate the imaging signal to the abundance of chromophore). Although there have been significant efforts relating to accuracy of PAI[134], there remains a paucity of data relating to precision. Biological validation of the sensitivity and specificity of the readout in relation to the target biological process should be made using *in vivo* models that recapitulate the human condition being studied. This review has revealed the near ubiquitous use of simple animal models, including subcutaneous tumors. Immunodeficient nude mice are also used routinely, which avoid the impact of skin melanin on optical absorption and minimize interactions with the immune system. While these systems provide an acceptable proof-of-concept, comparison between contrast agents would benefit from standardization (using published recommendations, e.g. by Dawidczyk *et al*[135]) with regard to the disease model, tumor sizes, time points and reported metrics. Translation of findings into transgenic mouse models on immune competent backgrounds (e.g. C57BL/6) will ultimately be needed for widespread uptake in preclinical research.

The exogenous contrast agents described here are still in the early stages of exploration. Opposing the current trend towards vast increases in the number of different signaling compounds available, we believe it is crucial to better understand the photophysical and biological properties of the classes that have already been reported. Lessons learned from other areas of molecular imaging indicate that focusing efforts on contrast agents that prove successful in more rigorous studies of biocompatibility and biological validation using realistic animal models of disease can help to accelerate widespread application. Future studies must also include comparisons to gold standards, either *in vivo* with other imaging modalities or *ex vivo* with histology. While challenging, if successful, these studies will likely aid the uptake of PAI as a tool in preclinical cancer biology and hence facilitate rapid clinical translation of PAI as a localized molecular imaging modality for personalized patient management.

Acknowledgments

We would like to thank Prof. Jeremy Baumberg from the Department of Physics in Cambridge for helpful discussions on gold nanoparticle LSPR. J.W. and S.E.B. are supported by: a CRUK Career Establishment Award (grant no. C47594/A16267); CRUK Core Funding (C14303/A17197); EU CIG (FP7-PEOPLE-2013-CIG-630729) and the EPSRC-CRUK Cancer Imaging Centre in Cambridge and Manchester (C197/A16465). PB receives support from King's College London and University College London Comprehensive Cancer Imaging Centre Cancer Research UK & Engineering and Physical Sciences Research Council, in association with the

Medical Research Council and Department of Health, UK and European Union project FAMOS (FP7 ICT, Contract 317744)

Figures

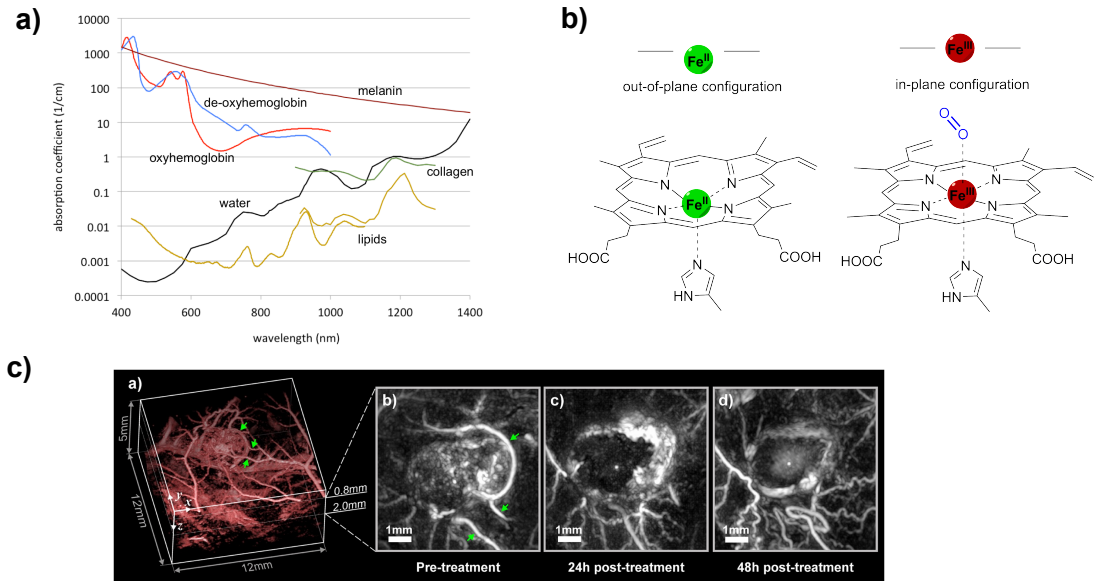

Figure 1. Photoacoustic imaging of endogenous chromophores.
a) Absorption spectra of the main endogenous light absorbing components. λ=584 nm and λ=797 nm are the isosbestic wavelengths where HbO_2 and Hb have identical molar extinction coefficients, enabling measurement of Hb_{total}. Oxyhemoglobin (HbO_2), red line (150 gl^{-1}); deoxyhemoglobin (Hb), blue line (150 gl^{-1}); water, black line[136] (80% by volume in tissue); lipid, yellow lines[137,138] (20% by volume in tissue); melanin, brown line (μ_a corresponds to that in skin); collagen, green line.
b) The different configurations of the heme group before and after oxygen binding leading to the characteristic changes in the absorption spectrum.
c) PAI (λ=640 nm) of tumor vasculature showing the effect of the vascular disrupting agent OXi4503.[6]
Data in (a) taken from http://omlc.ogi.edu/spectra/

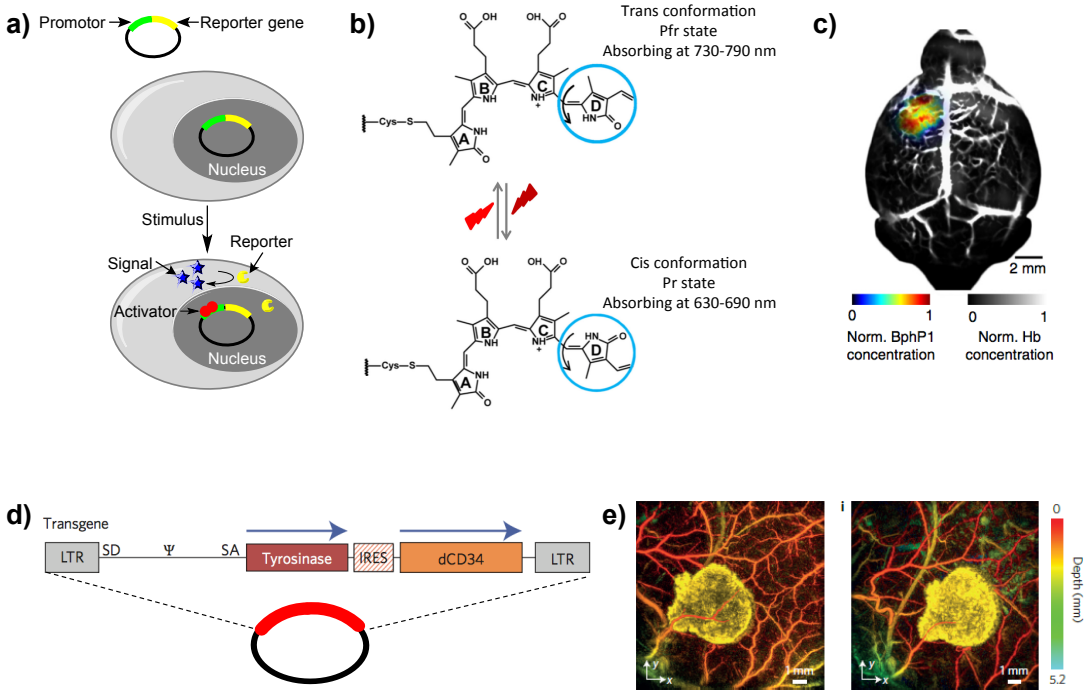

Figure 2. Photoacoustic imaging of genetically encoded chromophores.
a) Simplified schematic demonstration of a general enzymatic reporter gene construct.
b) Photoswitching chemistry of a Biliverdin chromophore from the Pfr state to the Pr state, and vice versa, induced by NIR (~730 – 790 nm) and far-red (~630 – 690 nm) light illumination, respectively.[22]
c) Deep PA computed tomography of mouse brain U87 tumor expressing BphP1, with the surrounding vasculature show in grayscale. The tumor (in color) was ~3mm beneath the scalp surface.[22]
d) Retroviral vector construct for stable transduction of cells for visualization of tyrosinase (Tyr) expression mammalian cells. (LTR: long terminal repeat, includes the promotor; SD: splice donor; ψ: viral packaging signal, which directs the incorporation of vector RNA into virions; SA: splice acceptor; IRES: internal ribosome entry sites).[24]
e) Serial longitudinal *in vivo* PA images of stable transduced, Tyr-expressing K562 cells after subcutaneous injection into the flank of a nude mouse, illustrating sensitive detection of produced melanin with depth resolution afforded by PAI (spatial resolution <100 µm at up to 10 mm depth).[24]

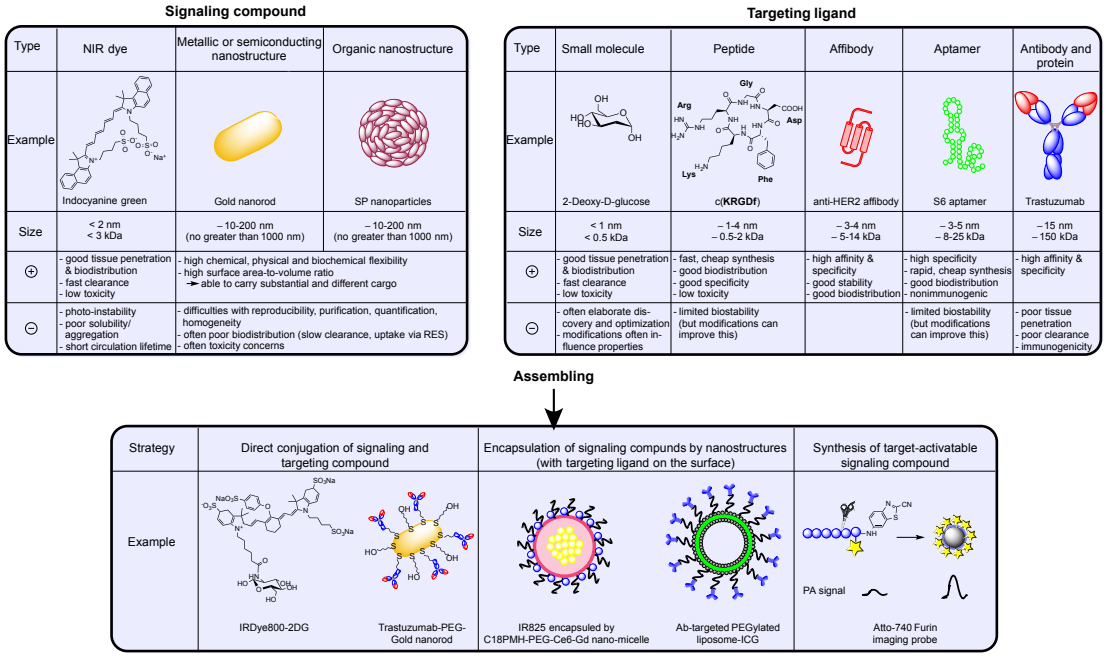

Figure 3. Assembly of molecular imaging contrast agents for PAI combining a signaling compound with a targeting ligand. Current strategies for the development of targeted contrast agents, are: the direct conjugation of signaling compounds with targeting ligands; encapsulation of signaling compounds (and targeting ligand) by nanostructures; or encapsulation (with targeting ligands) and synthesis of target-activatable signaling compounds. The targeting ligand and signaling compound should be compatible in their chemical, physical and biological properties. Examples of the relative advantages and disadvantages of each approach are indicated by +/-.[32,33,126,139,140]

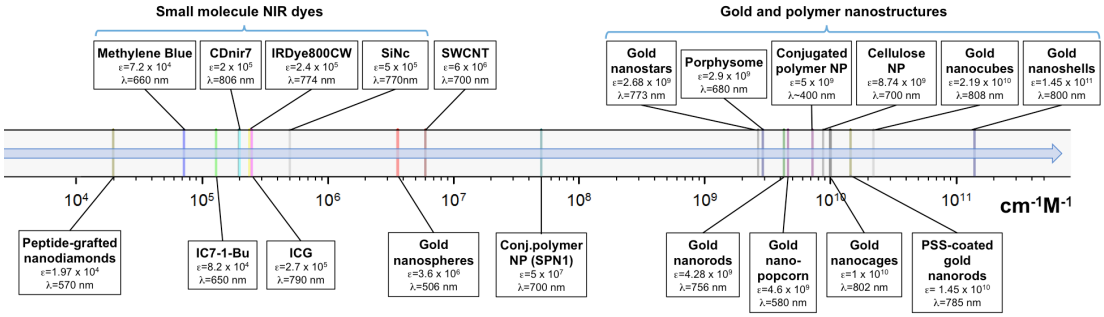

Figure 4. Schematic overview of the reported extinction coefficients of a selection of signaling compounds used for PAI:
Peptide-grafted nanodiamonds[87]; methylene blue[141]; IC7-1-Bu[142]; CDnir7[143]; IRDye800CW, ICG (http://www.spectra.arizona.edu/); SiNc[144]; gold nanospheres[145]; SWNTs[109]; SPN1[109]; gold nanostar[146]; porphysome[110]; gold nanorod[147]; gold nanopopcorn[148]; conjugated polymer NP[109]; cellulose NP[119]; gold nanocages[149]; PSS-coated gold nanorods[150]; gold nanocubes[151]; and gold nanoshells[152]. (λ represents the peak absorption wavelength).

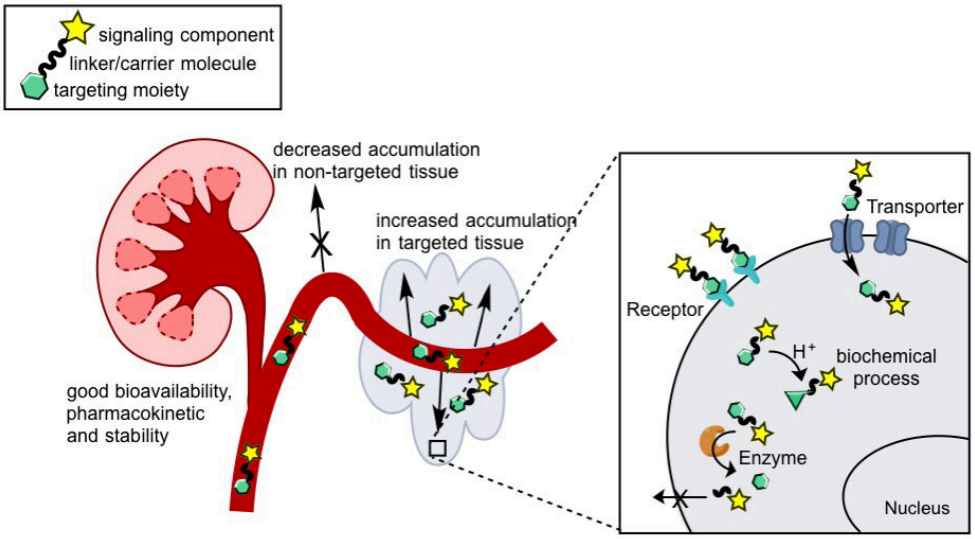

Figure 5. Physiological barriers encountered during molecular imaging.
Design of contrast agents for molecular PAI must consider both circulatory and cellular barriers, as well as the active targeting of cell surface receptors, transporters, metabolic enzymes or biochemical processes to provide the molecular readout.

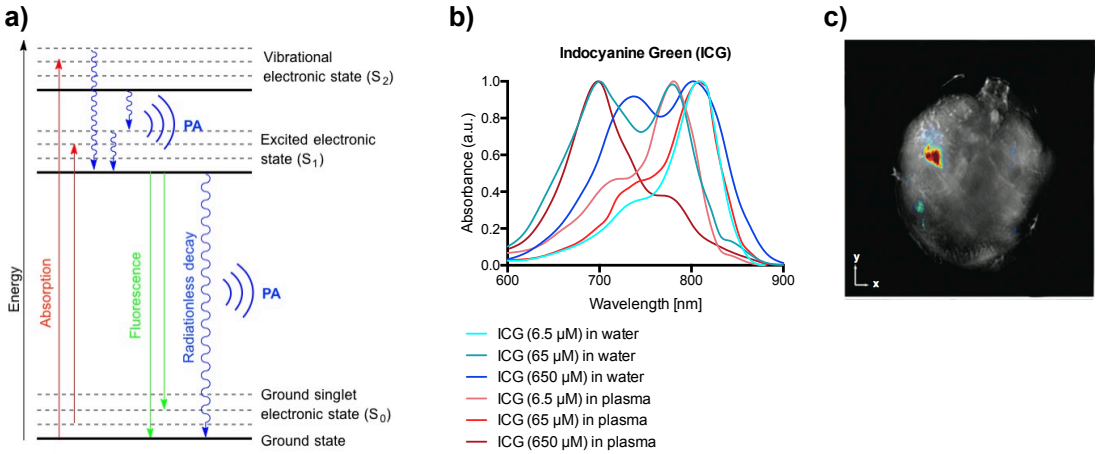

Figure 6. Optical properties of near infrared (NIR) small molecule dyes and application for imaging the extravascular target epidermal growth factor receptor (EGFR) in pancreatic cancer.

a) General Jablonski diagram showing energetic transitions for a NIR dye after optical excitation.

b) Example absorption spectra of ICG in water and plasma in different concentrations. The dye concentration and *in vivo* environment both significantly impact the spectral properties of small molecule dyes, which can be challenging for PAI studies (spectra data used from University of Arizona http://www.spectra.arizona.edu/)

c) Multispectral optoacoustic tomography (MSOT) of pancreatic adenocarcinoma from a mouse at 7 days post implantation using EGF-CF-750 at 6 hours postinjection.[64]

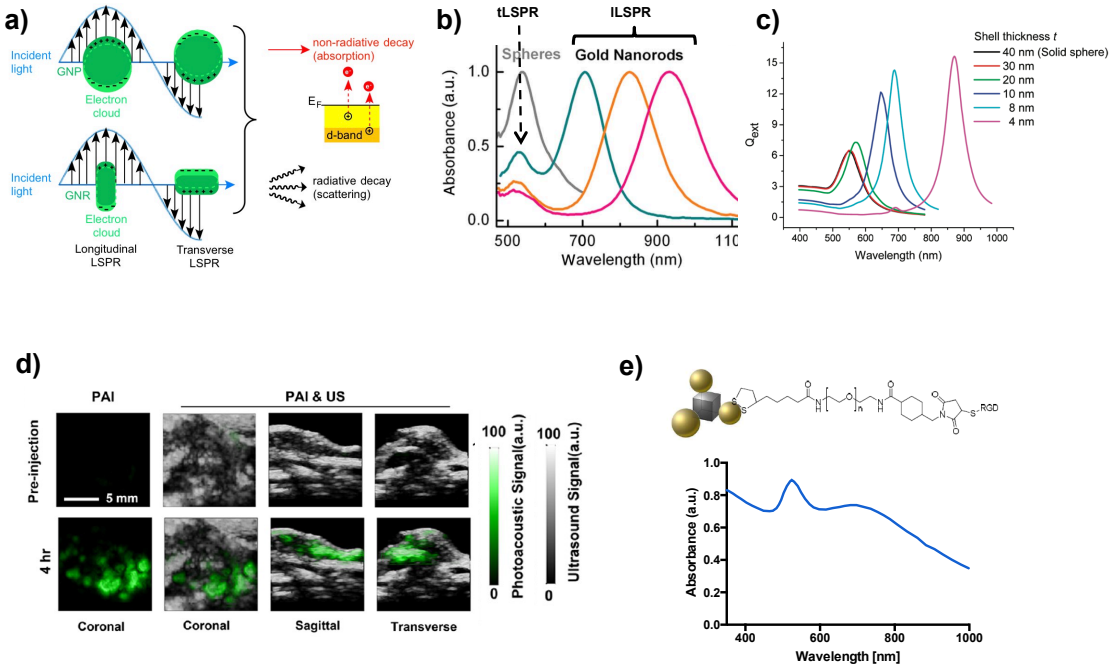

Figure 7. Optical properties of gold nanoparticles (GNP) and application for imaging the intravascular target $\alpha_v\beta_3$ integrin in glioma.

a) Localized surface plasmon resonance (LSPR) of spherical GNP and GNR: electromagnetic waves induce collective oscillation of the conduction electrons relative to the lattice of positive atomic cores (due to Coulomb interactions), which can be described as a bosonic quasiparticle, the plasmon. Plasmons can decay radiatively via re-emitting photons (scattering) or non-radiatively by e.g. transferring the energy to electrons leading to hot electron-hole pairs. The relaxation of the excited electrons leads to a partly conversion of the energy into heat, essential for PAI.[153,154]

b) Surface plasmon absorption spectra of gold nanorods of different aspect ratios, showing the sensitivity of the strong longitudinal band (longitudinal LSPR, lLPSR) to the aspect ratios of the nanorods (tLSPR = transverse LSPR). In comparison to GNR, gold nanospheres (grey line) show one peak absorption in green spectral range. (modified from ref.[155])

c) Surface plasmon resonance frequency of gold nanoshells can be tuned towards the NIR range by varying the shell thickness relative to the core size.[156]

d) PAI and ultrasound imaging of U87MG tumours in nude mice with intravenously injected $\alpha_v\beta_3$ integrin targeted gold tripods.[77]

e) Chemical structure and UV-Vis spectroscopic profile $\alpha_v\beta_3$ integrin targeted gold tripods.[77]

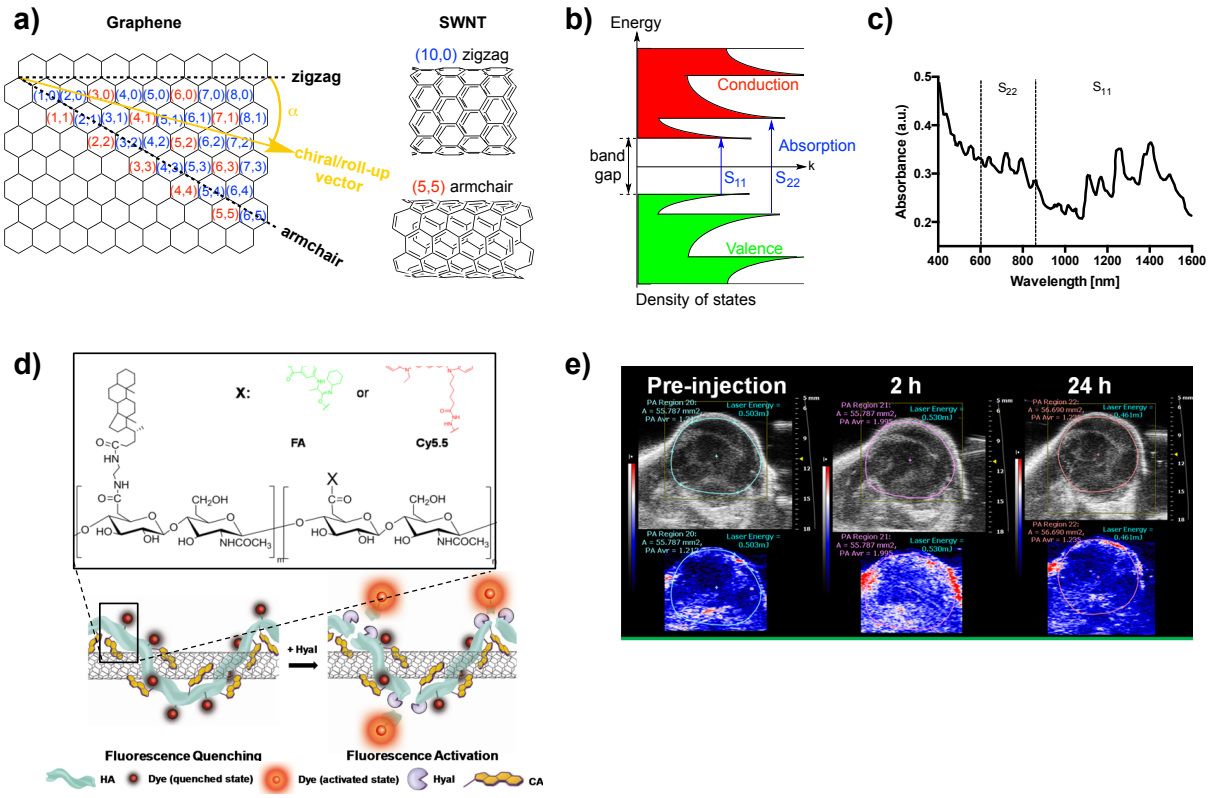

Figure 8. Optical properties of carbon nanotubes and application for imaging the extravascular target CD44 receptor in head and neck squamous cell carcinoma.
a) Schematic honeycomb structure of a single layer graphene sheet and structure of a semiconducting zigzag-single walled carbon nanotubes (SWNT) as well as a metallic armchair-SWNT. SWNT can be formed by rolling up the graphene sheet from lattice point (0,0) to (n,m) along a chiral (roll-up) vector; the vector's length indicates the circumference/diameter of the tube, the chiral angle (alpha) the tilt between the hexagonal lattice and that vector and thus the chirality. Depending on the nanotubes diameter and twist the SWNT can be metallic (red n,m numbers) or semiconducting (blue n,m numbers).
b) Schematic illustration of the density of states (DOS) with respect to energy for semiconducting SWNT. (k = wavevector, $S_{11/22}$ = first/second energy transition for semiconducting SWNT)
c) UV-vis-NIR absorption spectra of SDS-suspended HiPco SWNT showing the S_{11} and S_{22} regions. These spectra are of sodium dodecyl sulphate (SDS)- suspended HiPco SWNTs. Resolved peaks correspond to various (n, m) structures.[157]
d) Schematic illustration of dye-labeled hyaluronic acid-5beta-cholanic acid (HAC) conjugate and its activation of fluorescence properties. HAC wraps the SWNT due to hydrophobic interactions with cholanic acid, while the hydrophilic backbone provides solubility. In the attached form the fluorescence of the dye is quenched but in presence of hyaluronidase (Hyal) the dye molecules are released from the SWNT and fluorescence is recovered. (modified from ref.[86])
e) Ultrasound (top) and PAI (bottom) of the bottom hind limb SCC7 tumor of mice pre-injection and at 2 h and 20 h post-injection of Cy5.5-HAC-SWNT.[86]

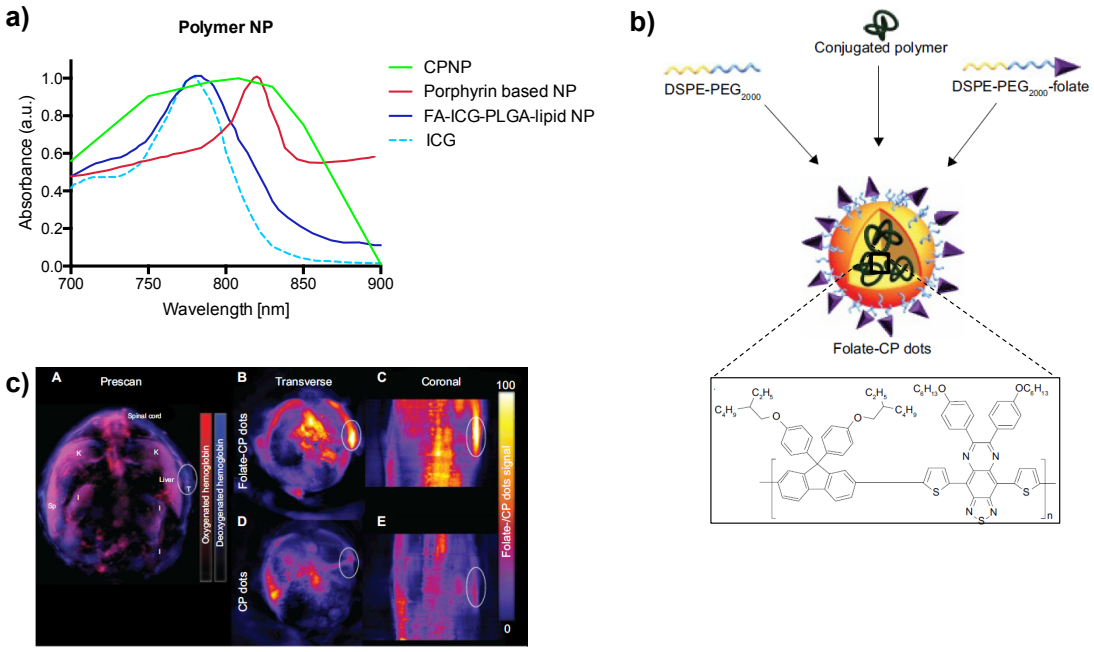

Figure 9. Optical properties of conjugated polymers and application to imaging the extravascular target folate receptor in breast cancer.
a) Absorption spectra of targeted conjugated polymer (green line) (shown in b and c) [108], porphyrin based NPs encapsulating perfluorocarbon gas (red line)[113], ICG (light blue, dashed line) and FA-ICG-PLGA-lipid polymer nanoparticle (PNP) (dark blue line)[122]. Conjugated polymers often possess a broadband absorption profile whereas the porphyrin based NPs show a narrow absorption peak in the NIR allowing a clearer identification in PAI. The absorption of PNPs with integrated signaling compounds show in general the characteristics of the chosen signaling compound (c.f. ICG and FA-ICG-PLGA-lipid PNP in a).
b) Schematic illustration of the structure of folate-CP dots including the conjugated polymer PFTTQ, DSPE-PEG$_{2000}$, and DSPE-PEG$_{2000}$-folate.[108]
c) PAI of mice bearing FR+ve MCF-7 breast cancer xenografts (A) before systemic administration of the probe, (B + C) 3 hours after administration of folate-CP dots and 3 hours after administration of untargeted CP-dots (D +E).[108]

Literature cited:

1. Ntziachristos, V. Going deeper than microscopy: the optical imaging frontier in biology. *Nat. Methods* **7,** 603–614 (2010).
2. Beard, P. Biomedical photoacoustic imaging. *Interface Focus* **1,** 602–31 (2011).
3. Taruttis, a., van Dam, G. M. & Ntziachristos, V. Mesoscopic and Macroscopic Optoacoustic Imaging of Cancer. *Cancer Res.* **75,** 1548–1560 (2015).
4. Zackrisson, S., van de Ven, S. M. W. Y. & Gambhir, S. S. Light In and Sound Out: Emerging Translational Strategies for Photoacoustic Imaging. *Cancer Res.* **74,** 979 – 1004 (2014).
5. Bohndiek, S. *et al.* Photoacoustic tomography detects early vessel regression and normalization during ovarian tumor response to the anti-angiogenic therapy Trebananib. *J. Nucl. Med.* **215,** (2015).
6. Laufer, J. *et al.* In vivo preclinical photoacoustic imaging of tumor vasculature development and therapy. *J. Biomed. Opt.* **17,** 056016 (2012).
7. Wang, L., Maslov, K. & Wang, L. V. Single-cell label-free photoacoustic flowoxigraphy in vivo. *Proc. Natl. Acad. Sci. U. S. A.* **110,** 5759–64 (2013).
8. Xu, Z., Li, C. & Wang, L. V. Photoacoustic tomography of water in phantoms and tissue. *J. Biomed. Opt.* **15,** 036019 (2010).
9. Oh, J.-T. *et al.* Three-dimensional imaging of skin melanoma in vivo by dual-wavelength photoacoustic microscopy. *J. Biomed. Opt.* **11,** 34032–1 – 34032–4 (2006).
10. Levi, J. *et al.* Molecular Photoacoustic Imaging of Follicular Thyroid Carcinoma. *Clin. Cancer Res.* **19,** 1494–1502 (2013).
11. Li, P.-C. *et al.* In vivo photoacoustic molecular imaging with simultaneous multiple selective targeting using antibody-conjugated gold nanorods. *Opt. Express* **16,** 18605–18615 (2008).
12. Luke, G. P., Myers, J. N., Emelianov, S. Y. & Sokolov, K. V. Sentinel lymph node biopsy revisited: Ultrasound-guided photoacoustic detection of micrometastases using molecularly targeted plasmonic nanosensors. *Cancer Res.* **74,** 5397–5408 (2014).
13. Guggenheim, J. a. *et al.* Photoacoustic imaging of human lymph nodes with endogenous lipid and hemoglobin contrast. *J. Biomed. Opt.* **20,** 050504 (2015).
14. Xu, Z., Zhu, Q. & Wang, L. V. In vivo photoacoustic tomography of mouse cerebral edema induced by cold injury. *J. Biomed. Opt.* **16,** 066020 (2011).
15. Zhang, H. F., Maslov, K., Stoica, G. & Wang, L. V. Functional photoacoustic microscopy for high-resolution and noninvasive in vivo imaging. *Nat. Biotechnol.* **24,** 848–851 (2006).
16. Stoffels, I. *et al.* Metastatic status of sentinel lymph nodes in melanoma determined noninvasively with multispectral optoacoustic imaging. *Sci. Transl. Med.* **7,** (2015).
17. Kang, J. H. & Chung, J.-K. Molecular-Genetic Imaging Based on Reporter Gene Expression. *J. Nucl. Med.* **49,** 164S–179S (2008).
18. Razansky, D. *et al.* Multispectral opto-acoustic tomography of deep-seated fluorescent proteins in vivo. *Nat. Photonics* **3,** 412–417 (2009).
19. Laufer, J., Jathoul, A., Pule, M. & Beard, P. In vitro characterization of genetically expressed absorbing proteins using photoacoustic spectroscopy. *Biomed. Opt. Express* **4,** 2477–90 (2013).

20. Shu, X. *et al.* Mammalian Expression of Infrared Fluorescent Proteins Engineered from a Bacterial Phytochrome. *Science (80-.).* **324,** 804–807 (2009).

21. Filonov, G. S. *et al.* Deep-tissue photoacoustic tomography of a genetically encoded near-infrared fluorescent probe. *Angew. Chemie - Int. Ed.* **51,** 1448–1451 (2012).

22. Yao, J. *et al.* Multiscale photoacoustic tomography using reversibly switchable bacterial phytochrome as a near-infrared photochromic probe. *Nat. Methods* 1–9 (2015). doi:10.1038/nmeth.3656

23. Cai, X. *et al.* Multi-scale molecular photoacoustic tomography of gene expression. *PLoS One* **7,** 1–7 (2012).

24. Jathoul, A. P. *et al.* Deep in vivo photoacoustic imaging of mammalian tissues using a tyrosinase-based genetic reporter. *Nat. Photonics* **9,** 239–246 (2015).

25. Qin, C. *et al.* Tyrosinase as a multifunctional reporter gene for Photoacoustic/MRI/PET triple modality molecular imaging. *Sci. Rep.* **3,** 1490 (2013).

26. Urabe, K. *et al.* The inherent cytotoxicity of melanin precursors: a revision. *Biochim. Biophys. Acta* **1221,** 272–278 (1994).

27. Tenzer, S. *et al.* Rapid formation of plasma protein corona critically affects nanoparticle pathophysiology. *Nat. Nanotechnol.* **8,** 772–81 (2013).

28. Lynch, I. & Dawson, K. a. Protein-nanoparticle interactions. *Nano Today* **3,** 40–47 (2008).

29. Lundqvist, M. Nanoparticles: Tracking protein corona over time. *Nat. Publ. Gr.* **8,** 1–2 (2013).

30. Petros, R. a. & DeSimone, J. M. Strategies in the design of nanoparticles for therapeutic applications. *Nat. Rev. Drug Discov.* **9,** 615–627 (2010).

31. Nie, L. *et al.* In vivo volumetric photoacoustic molecular angiography and therapeutic monitoring with targeted plasmonic nanostars. *Small* **10,** 1585–1593 (2014).

32. Chatni, M. R. *et al.* Tumor glucose metabolism imaged in vivo in small animals with whole-body photoacoustic computed tomography. *J. Biomed. Opt.* **17,** 076012 (2012).

33. Dragulescu-Andrasi, A., Kothapalli, S. R., Tikhomirov, G. a., Rao, J. & Gambhir, S. S. Activatable oligomerizable imaging agents for photoacoustic imaging of furin-like activity in living subjects. *J. Am. Chem. Soc.* **135,** 11015–11022 (2013).

34. Urano, Y. *et al.* Selective molecular imaging of viable cancer cells with pH-activatable fluorescence probes. *Nat. Med.* **15,** 104–109 (2009).

35. Tiede, C. *et al.* Adhiron: A stable and versatile peptide display scaffold for molecular recognition applications. *Protein Eng. Des. Sel.* **27,** 145–155 (2014).

36. Löfblom, J. *et al.* Affibody molecules: Engineered proteins for therapeutic, diagnostic and biotechnological applications. *FEBS Lett.* **584,** 2670–2680 (2010).

37. Sun, H. *et al.* Oligonucleotide aptamers: new tools for targeted cancer therapy. *Mol. Ther. Nucleic Acids* **3,** e182 (2014).

38. Olafsen, T. & Wu, A. M. Antibody Vectors for Imaging. *Semin. Nucl. Med.* **40,** 167–181 (2010).

39. Matsumura, Y. & Maeda, H. A new concept for macromolecular therapeutics in cancer chemotherapy: mechanism of tumoritropic accumulation of proteins and the antitumor agents Smancs. *Cancer Res.* **46,** 6387– 6392 (1986).

40. Clark, A. J. *et al.* CRLX101 nanoparticles localize in human tumors and not in adjacent, nonneoplastic tissue after intravenous dosing. *Proc. Natl. Acad. Sci.* **113,** 201603018 (2016).

41. Jaffe, H. H. & Miller, A. L. The fates of electronic excitation energy. *J. Chem. Educ.* **43,** 469–473 (1966).

42. Lin, Y., Weissleder, R. & Tung, C. H. Novel near-infrared cyanine fluorochromes: Synthesis, properties, and bioconjugation. *Bioconjug. Chem.* **13,** 605–610 (2002).

43. Song, F. *et al.* Syntheses, spectral properties and photostabilities of novel water-soluble near-infrared cyanine dyes. *J. Photochem. Photobiol. A Chem.* **168,** 53–57 (2004).

44. Kuebler, W. M. How NIR is the future in blood flow monitoring? *J. Appl. Physiol.* **104,** 905–906 (2008).

45. Philip, R., Penzkofer, a, Baumler, W., Szeimies, R. M. & Abels, C. Absorption and fluorescence spectroscopic investigation of indocyanine green. *J. Photochem. Photobiol. A-Chemistry* **96,** 137–148 (1996).

46. Landsman, M. L., Kwant, G., Mook, G. a & Zijlstra, W. G. Light-absorbing properties, stability, and spectral stabilization of indocyanine green. *J. Appl. Physiol.* **40,** 575–583 (1976).

47. Mordon, S., Devoisselle, J. M., Soulie-Begu, S. & Desmettre, T. Indocyanine green: physicochemical factors affecting its fluorescence in vivo. *Microvasc. Res.* **55,** 146–152 (1998).

48. Pauli, J. *et al.* An in vitro characterization study of new near infrared dyes for molecular imaging. *Eur. J. Med. Chem.* **44,** 3496–3503 (2009).

49. Umezawa, K., Citterio, D. & Suzuki, K. Water-soluble NIR fluorescent probes based on squaraine and their application for protein labeling. *Anal. Sci.* **24,** 213–217 (2008).

50. Sreejith, S., Carol, P., Chithra, P. & Ajayaghosh, A. Squaraine dyes: a mine of molecular materials. *J. Mater. Chem.* **18,** 264 (2008).

51. Kim, S. H. *et al.* Absorption spectra, aggregation and photofading behaviour of near-infrared absorbing squarylium dyes containing perimidine moiety. *Dye. Pigment.* **55,** 1–7 (2002).

52. Zhang, D. *et al.* Nano-Confined Squaraine Dye Assemblies: New Photoacoustic and Near-Infrared Fluorescence Dual-Modular Imaging Probes in Vivo. *Bioconjug. Chem.* **25,** 2021 – 2029 (2014).

53. An, F. *et al.* Aggregation-Induced Near-Infrared Absorption of Squaraine Dye in an Albumin Nanocomplex for Photoacoustic Tomography in Vivo. *Appl. Mater. Interfaces* (2014).

54. Sreejith, S., Joseph, J., Lin, M., Menon, N. V. & Borah, P. Near-Infrared Squaraine Dye Encapsulated Micelles for in Vivo Fluorescence and Photoacoustic Bimodal Imaging. *ACS Nano* **9,** 5695–5704 (2015).

55. Morgounova, E., Shao, Q., Hackel, B. J., Thomas, D. D. & Ashkenazi, S. Photoacoustic lifetime contrast between methylene blue monomers and self-quenched dimers as a model for dual-labeled activatable probes. *J. Biomed. Opt.* **18,** 56004 (2013).

56. Yao, J., Maslov, K., Hu, S. & Wang, L. V. Evans blue dye-enhanced capillary-resolution photoacoustic microscopy in vivo. *J. Biomed. Opt.* **14,** 054049 (2009).

57. Gabrielli, D., Belisle, E., Severino, D., Kowaltowski, A. J. & Baptista, M. S. Binding, aggregation and photochemical properties of methylene blue in mitochondrial suspensions. *Photochem. Photobiol.* **79,** 227–232 (2004).

58. Kim, C., Erpelding, T. N., Jankovic, L. & Wang, L. V. Performance benchmarks of an array-based hand-held photoacoustic probe adapted from a clinical ultrasound system

for non-invasive sentinel lymph node imaging. *Philos. Trans. R. Soc. A Math. Phys. Eng. Sci.* **369,** 4644–4650 (2011).

59. Kim, C., Song, K. H., Gao, F. & Wang, L. V. Sentinel Lymph Nodes and Lymphatic Vessels : Noninvasive Dual-Modality in Vivo Mapping by Using Indocyanine Green in Rats — Volumetric Spectroscopic Photoacoustic Imaging and Planar Fluorescence Imaging. *Radiology* **255,** 442–450 (2010).

60. Song, L., Kim, C., Maslov, K., Shung, K. K. & Wang, L. V. High-speed dynamic 3D photoacoustic imaging of sentinel lymph node in a murine model using an ultrasound array. *Med. Phys.* **36,** 3724–3729 (2009).

61. McMasters, K. *et al.* Sentinel lymph node biopsy for breast cancer: a suitable alternative to routine axillary dissection in multi-institutional practice when optimal technique is used. *J Clin Oncol.* **18,** 2560–2566 (2000).

62. Russo, A. *et al.* A decade of EGFR inhibition in EGFR-mutated non small cell lung cancer (NSCLC): Old successes and future perspectives. *Oncotarget* **6,** 26814–25 (2015).

63. Segovia-mendoza, M., González-gonzález, M. E., Barrera, D. & Díaz, L. Efficacy and mechanism of action of the tyrosine kinase inhibitors gefitinib , lapatinib and neratinib in the treatment of HER2-positive breast cancer : preclinical and clinical evidence. **5,** 2531–2561 (2015).

64. Hudson, S. V. *et al.* Targeted Noninvasive Imaging of EGFR-Expressing Orthotopic Pancreatic Cancer Using Multispectral Optoacoustic Tomography. *Cancer Res.* **74,** 6271–6279 (2014).

65. Duncan, R. & Gaspar, R. Nanomedicine(s) under the microscope. *Mol. Pharm.* **8,** 2101–2141 (2011).

66. Daniel, M. C. & Astruc, D. Gold Nanoparticles: Assembly, Supramolecular Chemistry, Quantum-Size-Related Properties, and Applications Toward Biology, Catalysis, and Nanotechnology. *Chem. Rev.* **104,** 293–346 (2004).

67. Chen, Y.-S. *et al.* Enhanced thermal stability of silica-coated gold nanorods for photoacoustic imaging and image-guided therapy. *Opt. Express* **18,** 8867–8878 (2010).

68. Willets, K. a & Van Duyne, R. P. Localized surface plasmon resonance spectroscopy and sensing. *Annu. Rev. Phys. Chem.* **58,** 267–297 (2007).

69. Petryayeva, E. & Krull, U. J. Localized surface plasmon resonance: Nanostructures, bioassays and biosensing-A review. *Anal. Chim. Acta* **706,** 8–24 (2011).

70. Link, S., Burda, C., Nikoobakht, B. & El-Sayed, M. a. Laser-Induced Shape Changes of Colloidal Gold Nanorods Using Femtosecond and Nanosecond Laser Pulses. *J. Phys. Chem. B* **104,** 6152–6163 (2000).

71. Cavigli, L. *et al.* Size Affects the Stability of the Photoacoustic Conversion of Gold Nanorods. *J. Phys. Chem.* **118,** 16140–16146 (2014).

72. Chen, Y. S. *et al.* Silica-coated gold nanorods as photoacoustic signal nanoamplifiers. *Nano Lett.* **11,** 348–354 (2011).

73. Preston, T. C. & Signorell, R. Growth and optical properties of gold nanoshells prior to the formation of a continuous metallic layer. *ACS Nano* **3,** 3696–3706 (2009).

74. Skrabalak, S. E. *et al.* Gold Nanocages: Synthesis, Properties and Applications. *Acc. Chem. Res.* **41,** 1587–1595 (2008).

75. Xie, H. *et al.* Integrin αvβ3-targeted gold nanoshells augment tumor vasculature-specific imaging and therapy. *Int. J. Nanomedicine* **6,** 259–269 (2011).

76. Fard, J. K., Jafari, S. & Eghbal, M. A. A Review of Molecular Mechanisms Involved in Toxicity of Nanoparticles. *Adv. Pharm. Bullrtin* **5,** 447–454 (2015).

77. Cheng, K. *et al.* Construction and validation of nano gold tripods for molecular imaging of living subjects. *J. Am. Chem. Soc.* **136,** 3560–3571 (2014).

78. Zhang, M., Yudasaka, M., Ajima, K., Miyawaki, J. & Iijima, S. Light-assisted oxidation of single-wall carbon nanohorns for abundant creation of oxygenated groups that enable Chemical modifications with proteins to enhance biocompatibility. *ACS Nano* **1,** 265–272 (2007).

79. Krueger, A. & Lang, D. Functionality is key: Recent progress in the surface modification of nanodiamond. *Adv. Funct. Mater.* **22,** 890–906 (2012).

80. He, H. & Gao, C. General approach to individually dispersed, highly soluble, and conductive graphene nanosheets functionalized by nitrene chemistry. *Chem. Mater.* **22,** 5054–5064 (2010).

81. Bahr, J. L. *et al.* Functionalization of carbon nanotubes by electrochemical reduction of aryl diazonium salts: A bucky paper electrode. *J. Am. Chem. Soc.* **123,** 6536–6542 (2001).

82. De La Zerda, A. *et al.* Family of enhanced photoacoustic imaging agents for high-sensitivity and multiplexing studies in living mice. *ACS Nano* **6,** 4694–4701 (2012).

83. Liu, Z., Robinson, J. T., Sun, X. & Dai, H. PEGylated Nano-Graphene Oxide for Delivery of Water Insoluble Cancer Drugs (b). *J Am Chem Soc* **130,** 10876–10877 (2008).

84. O'Connell, M. J. *et al.* Band gap fluorescence from individual single-walled carbon nanotubes. *Science* **297,** 593–596 (2002).

85. Shao, Y. *et al.* Graphene based electrochemical sensors and biosensors: A review. *Electroanalysis* **22,** 1027–1036 (2010).

86. Swierczewska, M. *et al.* A Facile, One-Step Nanocarbon Functionalization for Biomedical Applications. *Nano Lett.* **12,** 3613–3620 (2012).

87. Vial, S. *et al.* Peptide-grafted nanodiamonds: Preparation, cytotoxicity and uptake in cells. *ChemBioChem* **9,** 2113–2119 (2008).

88. Shi, J. *et al.* A tumoral acidic pH-responsive drug delivery system based on a novel photosensitizer (fullerene) for in vitro and in vivo chemo-photodynamic therapy. *Acta Biomater.* **10,** 1280–1291 (2014).

89. Avouris, P., Freitag, M. & Perebeinos, V. Carbon-nanotube photonics and optoelectronics. *Nat. Photonics* **2,** 341–350 (2008).

90. Carlson, L. J. & Krauss, T. D. Photophysics of individual single-walled carbon nanotubes. *Acc. Chem. Res.* **41,** 235–243 (2008).

91. Bachilo, S. M. *et al.* Structure-Assigned Optical Spectra of Single-Walled Carbon Nanotubes. *Science (80-.).* **298,** 2361–2366 (2002).

92. De la Zerda, A. *et al.* Carbon nanotubes as photoacoustic molecular imaging agents in living mice. *Nat. Nanotechnol.* **3,** 557–562 (2008).

93. Wang, C. *et al.* RGD-conjugated silica-coated gold nanorods on the surface of carbon nanotubes for targeted photoacoustic imaging of gastric cancer. *Nanoscale Reserach Lett.* **9,** 1–10 (2014).

94. Zerda, A. D. La *et al.* Ultrahigh sensitivity carbon nanotube agents for photoacoustic molecular imaging in living mice. *Nano Lett.* **10,** 2168–2172 (2010).

95. Tripodo, G. *et al.* Hyaluronic acid and its derivatives in drug delivery and imaging:

Recent advances and challenges. *Eur. J. Pharm. Biopharm. Off. J. Arbeitsgemeinschaft für Pharm. Verfahrenstechnik e.V* **97,** 400–16 (2015).

96. Kostarelos, K. The long and short of carbon nanotube toxicity. *Nat. Biotechnol.* **26,** 774–776 (2008).
97. Wick, P., Clift, M. J. D., Rösslein, M. & Rothen-Rutishauser, B. A brief summary of carbon nanotubes science and technology: A health and safety perspective. *ChemSusChem* **4,** 905–911 (2011).
98. Schipper, M. L. *et al.* A pilot toxicology study of single-walled carbon nanotubes in a small sample of mice. *Nat. Nanotechnol.* **3,** 216–221 (2008).
99. Saito, N. *et al.* Safe clinical use of carbon nanotubes as innovative biomaterials. *Chem. Rev.* **114,** 6040–6079 (2014).
100. Kaur, R. & Badea, I. Nanodiamonds as novel nanomaterials for biomedical applications: Drug delivery and imaging systems. *Int. J. Nanomedicine* **8,** 203–220 (2013).
101. Mochalin, V. N., Shenderova, O., Ho, D. & Gogotsi, Y. The properties and applications of nanodiamonds. *Nat. Nanotechnol.* **7,** 11–23 (2011).
102. Zhu, Y. *et al.* The biocompatibility of nanodiamonds and their application in drug delivery systems. *Theranostics* **2,** 302–312 (2012).
103. Seabra, A. B., Paula, A. J., De Lima, R., Alves, O. L. & Durán, N. Nanotoxicity of graphene and graphene oxide. *Chem. Res. Toxicol.* **27,** 159–168 (2014).
104. Nguyen, T.-Q., Martini, I. B., Liu, J. & Schwartz, B. J. Controlling Interchain Interactions in Conjugated Polymers: The Effects of Chain Morphology on Exciton−Exciton Annihilation and Aggregation in MEH−PPV Films. *J. Phys. Chem. B* **104,** 237–255 (2000).
105. Feng, L. *et al.* Conjugated polymer nanoparticles: preparation, properties, functionalization and biological applications. *Chem. Soc. Rev.* **42,** 6620–33 (2013).
106. Wu, C. *et al.* Bioconjugation of ultrabright semiconducting polymer dots for specific cellular targeting. *J. Am. Chem. Soc.* **132,** 15410–15417 (2010).
107. Zha, Z. *et al.* Biocompatible polypyrrole nanoparticles as a novel organic photoacoustic contrast agent for deep tissue imaging. *Nanoscale* **5,** 4462–7 (2013).
108. Balasundaram, G. *et al.* Molecular photoacoustic imaging of breast cancer using an actively targeted conjugated polymer. *Int. J. Nanomedicine* **10,** 387–397 (2015).
109. Pu, K. *et al.* Semiconducting polymer nanoparticles as photoacoustic molecular imaging probes in living mice. *Nat. Nanotechnol.* **9,** 233–9 (2014).
110. Lovell, J. F. *et al.* Porphysome nanovesicles generated by porphyrin bilayers for use as multimodal biophotonic contrast agents. *Nat. Mater.* **10,** 324–332 (2011).
111. Ng, K. K. *et al.* Stimuli-Responsive Photoacoustic Nanoswitch for In Vivo Sensing Applications. *ACS Nano* **8,** 8363–8373 (2014).
112. Huynh, E., Jin, C. S., Wilson, B. C. & Zheng, G. Aggregate enhanced trimodal porphyrin shell microbubbles for ultrasound, photoacoustic, and fluorescence imaging. *Bioconjug. Chem.* **25,** 796–801 (2014).
113. Huynh, E. *et al.* In situ conversion of porphyrin microbubbles to nanoparticles for multimodality imaging. *Nat. Nanotechnol.* **10,** 325–332 (2015).
114. Rivankar, S. An overview of doxorubicin formulations in cancer therapy. *J. Cancer Res. Ther.* **10,** 853–858 (2014).
115. Pan, D. *et al.* Molecular photoacoustic tomography with colloidal nanobeacons.

Angew. Chemie - Int. Ed. **48,** 4170–4173 (2009).

116. Pan, D., Pramanik, M., Wickline, S. a., Wang, L. V. & Lanza, G. M. Recent advances in colloidal gold nanobeacons for molecular photoacoustic imaging. *Contrast Media Mol. Imaging* **6,** 378–388 (2011).
117. Liu, J. *et al.* Conjugated polymer nanoparticles for photoacoustic vascular imaging. *Polym. Chem.* **5,** 2854 (2014).
118. Pan, D. *et al.* Rapid synthesis of near infrared polymeric micelles for real-time sentinel lymph node imaging. *Adv. Healthc. Mater.* **1,** 582–589 (2012).
119. Jokerst, J. V., Van de Sompel, D., Bohndiek, S. E. & Gambhir, S. S. Cellulose nanoparticles are a biodegradable photoacoustic contrast agent for use in living mice. *Photoacoustics* **2,** 119–127 (2014).
120. Miki, K. *et al.* Near-Infrared Dye-Conjugated Amphiphilic Hyaluronic Acid Derivatives as a Dual Contrast Agent for In Vivo Optical and Photoacoustic Tumor Imaging. *Biomacromolecules* **16,** 219–227 (2015).
121. Aoki, H., Nojiri, M., Mukai, R. & Ito, S. Near-infrared absorbing polymer nano-particle as a sensitive contrast agent for photo-acoustic imaging. *Nanoscale* **7,** 337–343 (2015).
122. Wang, H. *et al.* In vivo photoacoustic molecular imaging of breast carcinoma with folate receptor-targeted indocyanine green nanoprobes. *Nanoscale* **6,** 14270–14279 (2014).
123. Yang, K. *et al.* Visualization of protease activity in vivo using an activatable photo-acoustic imaging probe based on CuS nanoparticles. *Theranostics* **4,** 134–141 (2014).
124. Massoud, T. F. & Gambhir, S. S. Molecular imaging in living subjects: seeing fundamental biological processes in a new light. *Genes Dev.* **17,** 545–580 (2003).
125. Hembury, M. *et al.* Gold–silica quantum rattles for multimodal imaging and therapy. *Proc. Natl. Acad. Sci.* **112,** 1959–1964 (2015).
126. Gong, H. *et al.* Engineering of multifunctional nano-micelles for combined photothermal and photodynamic therapy under the guidance of multimodal imaging. *Adv. Funct. Mater.* 1–11 (2014). doi:10.1002/adfm.201401451
127. Xi, L. *et al.* Photoacoustic and fluorescence image-guided surgery using a multifunctional targeted nanoprobe. *Ann. Surg. Oncol.* **21,** 1602–9 (2014).
128. Zhang, L. *et al.* Activatable Hyaluronic Acid Nanoparticle as a Theranostic Agent for Optical / Photoacoustic Imaging-Guided Photothermal Therapy. *ACS Nano* **8,** 12250–12258 (2014).
129. Janib, S. M., Moses, A. S. & MacKay, J. A. Imaging and drug delivery using theranostic nanoparticles. *Adv. Drug Deliv. Rev.* **62,** 1052–1063 (2010).
130. Shahil, K. M. F. & Balandin, A. a. Thermal properties of graphene and multilayer graphene: Applications in thermal interface materials. *Solid State Commun.* **152,** 1331–1340 (2012).
131. Mou, J. *et al.* Ultrasmall Cu2-xS Nanodots for Highly Efficient Photoacoustic Imaging-Guided Photothermal Therapy. *Small* 1–9 (2015). doi:10.1002/smll.201403249
132. Onoe, S., Temma, T., Kanazaki, K., Ono, M. & Saji, H. Development of photostabilized asymmetrical cyanine dyes for in vivo photoacoustic imaging of tumors Development of photostabilized asymmetrical cyanine dyes for in vivo photoacoustic imaging of tumors. *J. Biomed. Opt.* **20,** 096006 (2015).

133. Reynolds, G., Reynolds, G., Drexhage, K. & Drexhage, K. Stable heptamethine pyrylium dyes that absorb in the infrared. *J. Org. Chem.* **42,** 885–888 (1977).

134. Cox, B., Laufer, J. G., Arridge, S. R. & Beard, P. C. Quantitative spectroscopic photoacoustic imaging: a review. *J. Biomed. Opt.* **17,** 061202 (2012).

135. Dawidczyk, C. M., Russell, L. M. & Searson, P. C. Recommendations for Benchmarking Preclinical Studies of Nanomedicines. *Cancer Res.* **75,** 4016–4020 (2015).

136. Hale, G. M. & Querry, M. R. Optical Constants of Water in the 200-nm to 200-microm Wavelength Region. *Appl. Opt.* **12,** 555–563 (1973).

137. Veen, R. L. P. van *et al.* Determination of visible near-IR absorption coefficients of mammalian fat using time- and spatially resolved diffuse reflectance and transmission spectroscopy. *J. Biomed. Opt.* **10,** 054004 (2005).

138. Tsai, C. L., Chen, J. C. & Wang, W. J. Near-infrared absorption property of biological soft tissue constituents. *J. Med. Biol. Eng.* **21,** 7–14 (2001).

139. Lozano, N., Al-ahmady, Z. S., Beziere, N. S., Ntziachristos, V. & Kostarelos, K. Monoclonal antibody-targeted PEGylated liposome-ICG encapsulating doxorubicin as a potential theranostic agent. *Int. J. Pharm.* (2014). doi:10.1016/j.ijpharm.2014.10.045

140. Eghtedari, M. *et al.* Engineering of hetero-functional gold nanorods for the in vivo molecular targeting of breast cancer cells. *Nano Lett.* **9,** 287–91 (2009).

141. Ashkenazi, S. Photoacoustic lifetime imaging of dissolved oxygen using methylene blue. *J. Biomed. Opt.* **15,** 040501 (2010).

142. Onoe, S., Temma, T., Shimizu, Y., Ono, M. & Saji, H. Investigation of cyanine dyes for in vivo optical imaging of altered mitochondrial membrane potential in tumors. *Cancer Med.* **3,** 775–86 (2014).

143. Kang, N.-Y. *et al.* A macrophage uptaking near-infrared chemical probe for in vivo imaging of inflammation. *Chem. Commun. (Camb).* **50,** 6589–91 (2014).

144. Beziere, N. & Ntziachristos, V. Optoacoustic Imaging of Naphthalocyanine: Potential for Contrast Enhancement and Therapy Monitoring. *J. Nucl. Med.* **56,** 323–328 (2014).

145. Liu, X., Atwater, M., Wang, J. & Huo, Q. Extinction coefficient of gold nanoparticles with different sizes and different capping ligands. *Colloids Surf. B. Biointerfaces* **58,** 3–7 (2007).

146. de Puig, H., Tam, J. O., Yen, C.-W., Gehrke, L. & Hamad-Schifferli, K. Extinction Coefficient of Gold Nanostars. *J. Phys. Chem. C* **119,** 17408–17415 (2015).

147. Jokerst, J. V., Cole, A. J., Van De Sompel, D. & Gambhir, S. S. Gold nanorods for ovarian cancer detection with photoacoustic imaging and resection guidance via Raman imaging in living mice. *ACS Nano* **6,** 10366–10377 (2012).

148. Beqa, L., Fan, Z., Singh, A. K., Senapati, D. & Ray, P. C. Gold nano-popcorn attached SWCNT hybrid nanomaterial for targeted diagnosis and photothermal therapy of human breast cancer cells. *ACS Appl. Mater. Interfaces* **3,** 3316–3324 (2011).

149. Srivatsan, A. *et al.* Gold nanocage-photosensitizer conjugates for dual-modal image-guided enhanced photodynamic therapy. *Theranostics* **4,** 163–174 (2014).

150. Leonov, A. P. *et al.* Detoxification of gold nanorods by treatment with polystyrenesulfonate. *ACS Nano* **2,** 2481–2488 (2008).

151. Hu, J. *et al.* Theranostic Au cubic nano-aggregates as potential photoacoustic contrast and photothermal therapeutic agents. *Theranostics* **4,** 534–545 (2014).

152. Lu, W. *et al.* Effects of photoacoustic imaging and photothermal ablation therapy mediated by targeted hollow gold nanospheres in an orthotopic mouse xenograft model of glioma. *Cancer Res.* **71,** 6116–6121 (2011).

153. Clavero, C. Plasmon-induced hot-electron generation at nanoparticle/metal-oxide interfaces for photovoltaic and photocatalytic devices. *Nat. Photonics* **8,** 95–103 (2014).

154. Brongersma, M. L., Halas, N. J. & Nordlander, P. Plasmon-induced hot carrier science and technology. *Nat. Publ. Gr.* **10,** 25–34 (2015).

155. Li, J., Guo, H. & Li, Z. Microscopic and macroscopic manipulation of gold nanorod and its hybrid nanostructures. *Photonics Res.* **1,** 28–41 (2013).

156. Jain, P. K. & El-Sayed, M. a. Universal scaling of plasmon coupling in metal nanostructures: extension from particle pairs to nanoshells. *Nano Lett.* **7,** 2854–8 (2007).

157. Hodge, S. a., Bayazit, M. K., Coleman, K. S. & Shaffer, M. S. P. Unweaving the rainbow: a review of the relationship between single-walled carbon nanotube molecular structures and their chemical reactivity. *Chem. Soc. Rev.* **41,** 4409 (2012).